Removal of Environmental Effects in Structural Health Monitoring Data

Master Thesis

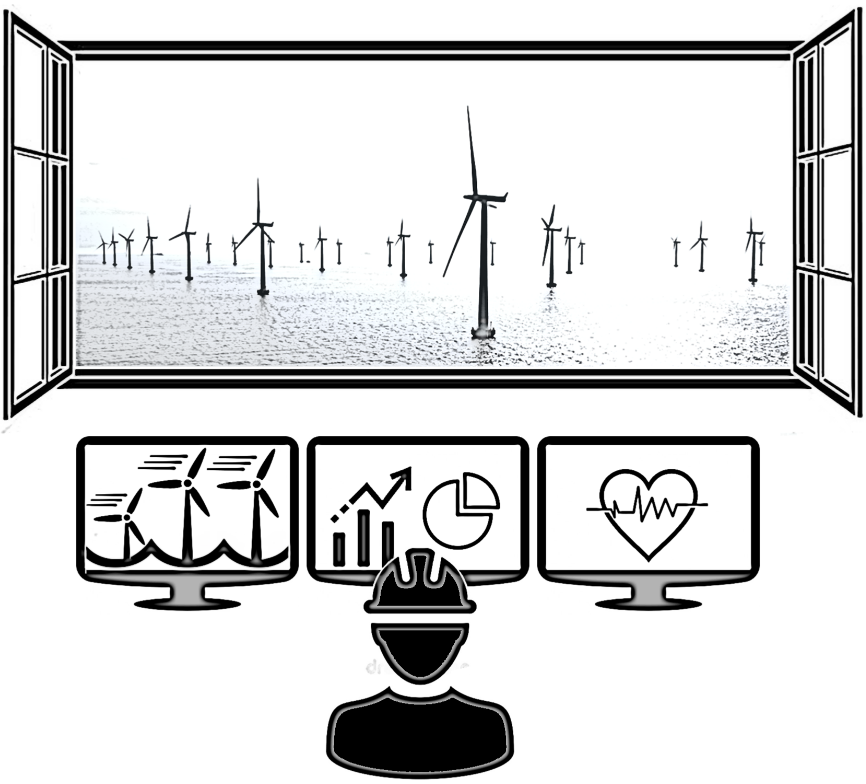

Tuan Viggo Luong Vo
Aalborg University, Esbjerg Department
M.Sc. in Engineering, Mechanical Design
June 2018

Title Page

Project title:	Removal of Environmental Effects in Structural Health Monitoring Data
Project theme:	Structural Health Monitoring
Project period:	5th of February to 7th of June 2018
Author:	Tuan Viggo Luong Vo
University:	Aalborg Universitet, Esbjerg Department
Field of study:	Master of Science in Mechanical Design
Supervisors:	Lars Damkilde & Martin Dalgaard Ulriksen
Number of pages:	60 (83 including Appendices)

Tuan Viggo Luong Vo

Date and signature

Abstact

The wind energy sector has, in recent decades, been expanding by multiple orders of magnitude due to a global desire of replacing finite energy sources with renewable and clean alternatives. The maturity of wind technology, its stable infrastructure and the cost-effectiveness are factors that motivate engineers to research and develop innovative solutions leading to overall improvements. While the volume of installations, power capacities, physical sizes and offshore placements are all increasing, it is obvious, that the ability to ascertain and ensure the structural integrity of wind turbines is becoming more challenging and more valuable. A demand for a more sophistical approach, with higher capability as well as reliability than conventional visual inspection, is clarified. This project focuses on a research to facilitate the development of a remote structural health monitoring system for wind turbines, of which, particularly, wind turbine blades are evaluated to be the preferred candidate of interest.

One major issue, prohibiting the development and implementation of a health monitoring system for wind turbine blades, is the confounding influences of environmental effects upon the sensitivity to identify the occurrence of damage. A reliable SHM system must be able to distinguish between changes caused by ambient variations, such as temperature fluctuations, and those caused by damage. This problem of data normalization, which can be ascertained by singling out a damage-sensitive feature from latent environmental influences, is the main focus point to be addressed in this particular thesis context. The employed approach, to remove environmental effects in SHM data, is based on a technique originating from the field of econometrics, namely cointegration. Non-stationary time series with common trends are considered as cointegrated if a linear combination of the series exists to be stationary. This residual linear combination will be purged from all common trends, thus, from an engineering perspective, this technique can be used to analyze whether or not, the environmental effects will be removed in the process of cointegration.

An experimental campaign of a full-scale operational Vestas V27 wind turbine has provided a substantial amount of empirical data. Over approximately a period of three months, this turbine was monitored and subjected to five different structural states including artificially introduced damages. Simultaneously, meteorological data from a nearby weather mast were collected. Hence, this campaign and its results provide the opportunity for the author of this thesis, to perform analyses and validate the inherent algorithms. The damage detection technique, which will be used to validate the robustness of the developed feature against environmental variations, is established by means of outlier analysis based on Mahalanobis metric.

Preface

This report represents the product of a master thesis of 30 ECTs, in the time period from 05-02-2018 to 07-06-2018. The thesis is written during fourth semester of the master programme in Mechanical Engineering at Aalborg University, Esbjerg Department. With the underlying theme to be 'Structural Health Monitoring', the project addresses one major issue prohibiting the implementation of a reliable health monitoring system for wind turbines: the confounding influences of environmental effects upon the sensitivity to identify the occurrence of damage. The concept of cointegration, originating from the field of econometrics, will be adapted to process structural health monitored data, with the intention to purge out environmental effects, and provide robust features for damage identification.

The theoretical principles and methods elaborated and applied in this report, which at some level are in accordance with the study curriculum, are elements within the formal subjects such as structural dynamics, finite element analysis, signal processing, statistics, calculus and linear algebra. It will be an advantage for the reader to have a certain degree of literacy concerning these subjects. Furthermore, the algorithms created during the project are in the format of Matlab-scripts, i.e. '.m'-files, one might have to gain access to the software, in order to open and review the mathematical procedures in this specific programming language. An enclosed CD is attached on page VII, in which the scripts as well as a PDF-version of the report is included.

A great extent of monitored data, collected from an experimental campaign of a full-scale operational Vestas V27 wind turbine in 2015, have prompted the opportunity for the author of this thesis, to perform numerical analyses based on empirical data. The author would like to express gratitude to; Lars Damkilde (project supervisor), Martin D. Ulriksen (project supervisor), Dmitri Tcherniak and Lasse L. Moelgaard all whom have been among the responsible of the campaign and authors of associated papers containing significant information regarding the experimental details. Furthermore, the project supervisors deserves to be acknowledged for their guidance throughout the project.

References to secondary sources such as research papers, books and websites are indicated with a simple numbering system and marked with square brackets, e.g. [1], which refers to the 1st position and can be found in the "Bibliography" section, starting from page 61. Relevant information such as the author(s), title, publisher, edition and year of publication will be informed, and for website references, the url-link and accessed date will be included. Figures from secondary sources be referenced in the associated caption text, thus, figures without references are produced by the author. Figures and equations are similarly numbered for convenience and reference purposes, where equations are marked with round brackets, e.g. (1.1), in which case the equation is to be found in chapter 1.

Table of Contents

Chapter 1

Introduction

The attention to renewable energy sources has been prevailing in recent decades because of an increasing awareness and concern of environmental problems and climate change issues induced by traditional energy sources. Due to the global desire of replacing finite energy sources with renewable alternatives as well as the industrial development and population growth, the demand of clean energy has been emerging rapidly. The European Union seeks to cover 20 % of its energy needs from renewable alternatives by 2020 [1]. Wind energy, among other renewable energy sources, is considered as one of the most substantial source and as a strong contender due to the maturity of the technology, the relative cost competitiveness and the stable infrastructure. In order to comply with the demand, and to harvest wind energy more efficiently due to cost-effective considerations, the numbers of wind turbines have been increasing as well as the sizes have become physically larger, making maintaining and repairing more challenging and expensive. In addition to these progressing developments, the installation sites for wind farms have been expanding from onshore to offshore, in deeper waters further from shore where the wind speeds are likely greater and more beneficial while the limitations as well as space and transport issues are less constricted.

For now, the world's currently most powerful wind turbine in serial production is the latest version of the MHI Vestas V164 [2] [3] with the blade length of 80 meters and power production capacity of 9.5MW. This is an impressive boost considering that many modern offshore turbines in use today are in the range of 4 to 6 MW. Originally, the V164's rated capacity was 7 MW in 2011, before its prototype was revealed in 2014 at Oesterild, northern Denmark, where the rated output capacity increased to 8 MW. Later that year, a remarkable event occurred due to favorable winds that allowed the turbine to sustain its rated capacity for 24 hours continuously: the one-day energy production record was set with the magnitude of 192 MWh [4]. Last year, in 2017, an upgraded version of the turbine with increased capacity, the V164-9MW, yet again, proved to sustain its rated capacity and set the record with an energy production of 216 MWh in 24 hours [5]. Notice, that only considerable turbines, in terms of tested, in serial production and industrialized, have been included in this context. It is known, that larger and potentially more efficient turbines are in advancement, such as the Halidade-X 12MW from GE renewable energy with blade lengths of 107 meters [6], or the most extreme-sized turbine found to date, the Segmented Ultralight Morphling Rotor (SUMR) Turbine of 50 MW and 200-meter blades from Sandia Lab (USA) [7] [8] [9]. As the size of power and wind turbines grow, the value of turbines correspondingly increase, the cost of interruptions and failures are likewise becoming greater whereas structural integrity inspections to ensure the reliability become more challenging. The bottom line is, that the ability of detecting upcoming as well as ongoing failures are becoming more necessary and more valuable, making the development of automated structural health monitoring systems particularly attractive in this industry.

1.1 Wind Turbine Related Accidents

According to accident statistics, collected from documented cases of worldwide wind turbine related accidents, by Caithness Windfarm Information Forum (CWIF) [10], in the time span of approximately 22 years, from 1996 to the 31st of March 2018, it is indicated that the biggest amount of incidents included was accounted and marked as blade failure. A number of 381 separate incidences, marked as blade failure, out of a total number of 2199 accidents, i.e. 17.3 % of the accidents were accounted as blade failure. A histogram illustrating the annual accident statistics of all included accidents and the blade failure number of accidents, is presented in Figure 1.1.

The second most common accident cause was fire with 316 counts corresponding to 14.4 % and the third most common was structural failure, which includes storm and lightning damages, poor quality control, lack of maintenance and component failure, with 197 counts corresponding to 9.0 %. Other categories of accident types are fatal accidents, human injury, human health, ice throw, transport, environmental damage and miscellaneous. It is important to keep in mind, that the categorizations do not duplicate in numbers except for the category of fatal since some accidents have caused multiple fatalities. Hence, the category of blade failure only refers to situations with failures directly and obviously connectable to the blade, meaning that accidents or failures that have been initiated by, for

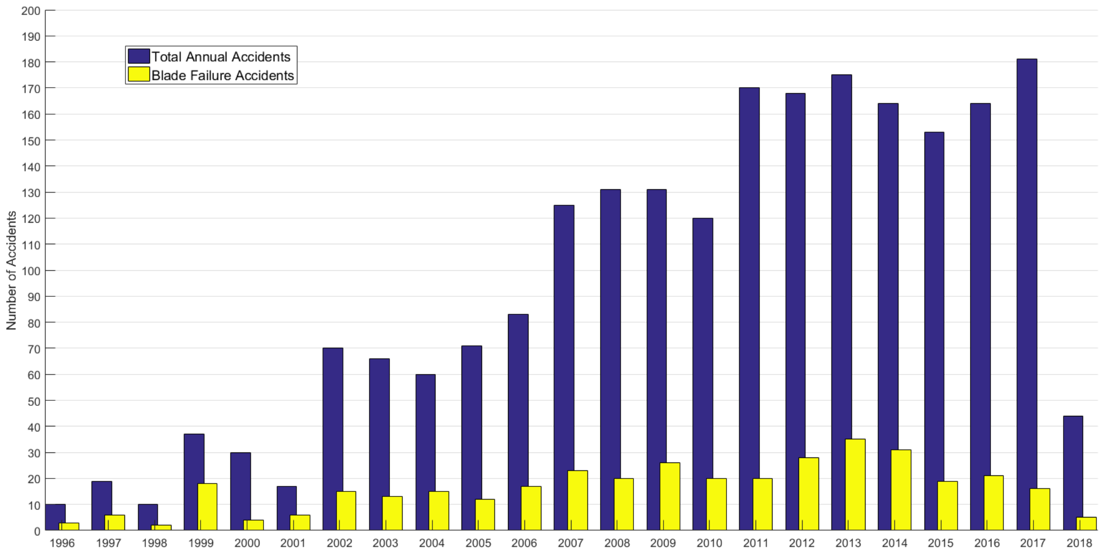

Figure 1.1: Annual histogram plot of wind turbine related accidents from 1996 to 31st of March 2018

instance, blade imbalances creating undesired vibrations to the gearbox or the whole structure leading to a complete collapse, or a blade failure leading to a human injury, might respectively fall under the category of structural failure and human injury instead of blade failure. An example of this is one structural failure included in the CWIF statistics about one year ago: A normally working turbine collapsed surprisingly on the 11th of May 2017 in Kansas with no obvious reason, despite the fact of an inspection procedure was performed the morning of the same day, see Figure 1.2, [11] [12]. Since no apparent reasons for the cause of collapse were concluded, CWIF marked it as an accident due to a structural failure. It might as well could have been a damageon the blade leading to the collapse. This means, hypothetically, that the percentage of blade failure most likely would be greater if all blade influenced accidents could be included in the category.

As more turbines are built, more accidents occur. This statement is supported by the statistical data summarized in the presented histogram, Figure 1.1. Notice that the data only ranges to the 31st of March 2018 Meaning that the last 9 months of 2018 is not accounted for in the histogram. The trend of increasing accidents underlines the fact of a need for a more reliable method to monitor the structural health of wind turbines, and thereby minimizing the consequences and ultimately prevent premature structural failures and associated accidents from happening.

Keep in mind that the statistical data provided by CWIF do not represent the

Figure 1.2: Premature Wind Turbine Collapse in Kansas 11th of May 2017 [11] [12]

.

entire history of worldwide wind turbine accidents. Only published and well documented accidents chosen by CWIF are included. The countries involved consist of the USA, Canada, Mexico, Puerto Rico, Nicaragua, Brazil, Afrika, UK, Ireland, Faroe Islands, Denmark, Norway, Sweden, Finland, Germany, Netherlands, Belgium, France, Spain, Portugal, Italy, Austria, Switzerland, Romania, Bulgaria, Turkey, Greece, Crete, China, Japan, Taiwan, Philippines, India, Australia and New Zealand. A full list of the accidents and the associated data including the origin country, date, description and details, info sources and website references can be found in the compendium compiled by CWIF [13].

A secondary source, GCube, provider of renewable energy insurance services, has in 2013 published a report summarizing the most common wind energy insurance claims made in the United States in 2012. The report shows that blade damage and gearbox failure were the two most common issues, accounting for respectively 41.4 % and 35.1 % of the cases and the top two causes were cited as poor maintenance with 24.5 % and lightning strikes with 23.4 % [14]. In 2015, an article published by Windpower Monthly referred to a research presented by the same company, GCube, which estimated that wind turbine rotor blades are failing at a rate of around 3.800 a year [15].

The two independent sources, CWIF and GCube, implicate that blade failures constitute as the most common concern regarding accidents of wind turbines. In addition to that, an experimental study from 2005 conducted by Khan MM, Iqbal MT and Khan F [16], has provided a reliability analysis of the respective components of a small scale wind turbine, i.e estimates of the reliability and failure rate of the tip break, yaw bearing, blades, bolts, hub, generator, gearbox, parking brakes, tower and anchor bolts. The results of the study show that the blades were among the most sensitive components with lowest reliability and subjected to potential failures. Taking the accident statistics as well as the experimental study into account, it can be concluded, that wind turbine blades are the most vulnerable component requiring attention, therefore, an excellent candidate to be investigated and monitored more frequently. Thus, the main components of focus in the upcoming chapters throughout the report will be wind turbine blades.

1.2 Visual Inspection of Wind Turbines

Conventional approaches to inspect the structural integrity of wind turbine blades typically consist of periodic visual inspections carried out by rope, platform, sky climber, drone, crane or lift access which demands temporarily interruptions of the turbine, i.e. temporarily stopping the production of electricity. The aim of visual inspection is to detect deterioration at a stage early enough to guarantee adequate safety and low costs of reconstruction. Obviously, performing inspection and repair is known to be more profitable than demolition and total replacement. An example of the approach, is for instance an inspection team from LM Power using ropes is presented in Figure 1.3.

These inspection methods require special equipments and highly trained technicians with proper expertise. Despite the fact of scheduling during low- or even non-productive seasons, this traditional process of visual inspection is still, both time demanding, risky in terms of safety issues and extremely costly. The uncertainties due to human errors, issues such as inaccessible areas and decreased vision due to the angle of perspective, fog and weather etc. are all factors that influence the quality of this type of inspection. Large surface damages, leakings and corrosion defects are likely visible and therefore detectable, whereas, for instance, subsurface and minor cracks induced by long term fatigue propagation can be almost impossible to be discovered by the human eye or by means of high resolution cameras and associated drones and image analysis software. In

Figure 1.3: Visual inspection of wind turbine performed by specially trained rope team from LM Wind Power [17]

fact, according to published reports of the offshore wind as well as the offshore oil industry, some wind turbine and platform accidents have occurred relatively a short time after the period of scheduled inspection. It has been discovered in some cases, that existing cracks, which led to total failure, were present during the scheduled visual inspection prior to these accidents, i.e. fatal cracks remained unnoticed during inspection. An example of this is the accident in Kansas, where the turbine passed inspection the morning of the collapse [11] [12]. This implicates inaccuracies and incomprehensiveness of the traditional visual inspection methods which emphasizes the concern, that there is a need for a more reliable alternative to continuously monitor the structural health of wind turbines.

1.3 Overview of Blade Design

In general, detailed information regarding the material, geometrical design and manufacturing processes of specific blades are kept confidential and not publicly available, due to rivalry among wind turbine manufacturers. The information presented in this present section, and the following section, 1.4, are based on studies concerning wind turbine materials as well as studies with wind turbines subjected to structural testing, referring to [18], [19] and [20].

Wind turbine blades and nacelles are generally made of fiber-reinforced composite materials, whereas generators and towers are manufactured from metals. The most important composite based parts of a turbine are the blades which also constitute to the highest cost among all components [21]. The airfoil geometry of a blade plays a major role, since it is responsible to capture and transmit aerodynamic forces into rotational torque in order for the generator to convert the energy and produce power. Thus, the high complexity and requirements for the blade material and design. A typical blade consists of webs in between two shells as illustrated in Figure 1.4.

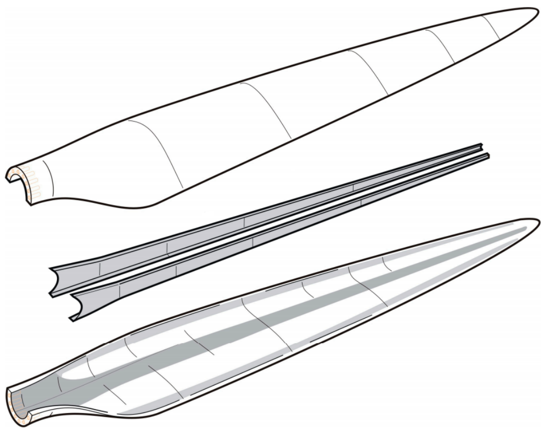

Figure 1.4: Illustration of the main sub-components of a wind turbine rotor blade, consisting of two aerodynamic shells and two shear webs [18]

.

The aerodynamic shells are the largest sub-components of a blade and is often primarily designed against elastic buckling. In order to reduce the weight, the shells are made of sandwich composite structures, i.e. composite sheets enclosing a sandwich core which is made from light-weight material such as polymer foam. The webs (sometimes one web, several webs, or a beam structure) inside of the blade, are the main load-carrying sub-component which are made with relatively high load capacity and fatigue resistant composite material such as glass- or carbon fiber. The surfaces of a blade are usually referred to as the upwind-/pressure side and the downwind-/suction side, whereas the edges are namely the trailing- and the leading edge. The root is located at the inner end of the blade, where the shape is more circular than the rest in order to fit and be mounted on the nacelle. The opposite end is referred as the tip of the blade. A cross-section of a general blade is depicted in Figure 1.5

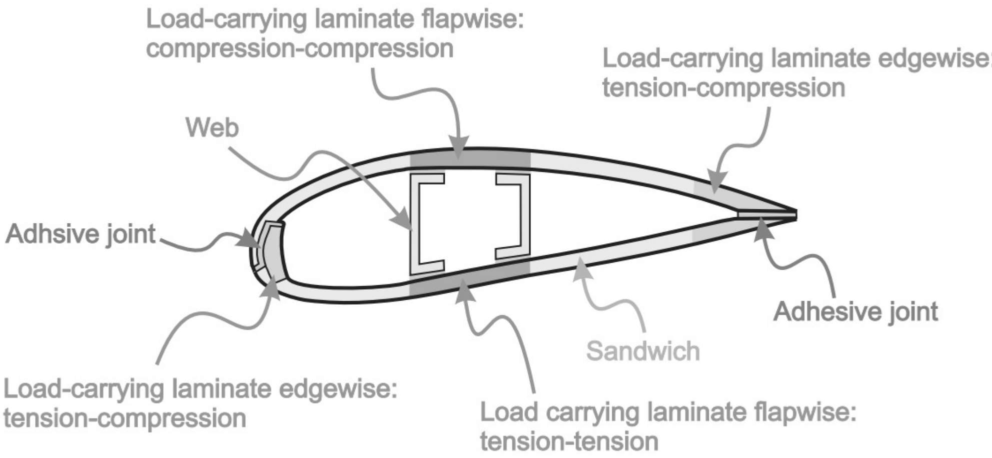

Figure 1.5: Cross-sectional view of the inner sub-components of a blade [18]

.

Wind pressure during operation causes loads on the faces, referred as flapwise load in Figure 1.5. The type of the loads are, respectively, compression-compression and tension-tension on the upwind side and on the downwind side, i.e. the reason for the terminology of pressure and suction sides. As for the edges, the load cycles between tension-compression, which is mainly caused by gravitational forces and torque loads. Other possible loads during operation are for instance temperature variations, rain erosion or more extraordinary; lightning strikes and extreme wind loads. Due to these various types of cycling loads at different locations on the blade, it is often realized, that different types of material for different parts of the blade could be advantageous. For ensuring the erosion-resistance of the blades, coating is essential, and the materials conventionally used for this purpose include epoxy and polyurethane gelcoats, polyurethane paint systems and tapes.

The power, size and volume of wind turbines are growing extensively and the current developments allow location sites further off shore than ever. Capacities above 10 MW (over 10.000 households), rotor blades exceeding 100 meters in length, and wind farms consisting of several hundred individual turbines, and yet, the trend of increasing is still ongoing. Due to this trend of increase in size and offshore placements, leading to the processes of upscaling and optimization the components, the material requirements are correspondingly increasing. Currently, a lot of active research are put in the development of alternative materials which are more damage resistant with higher strength, faster to produce, more favorable to the environment and recyclable. The stiffness, tensile and compression strength of the composite are controlled by the material properties of the reinforced fibers and their volume content. Alternative materials, other than glass- and carbon fiber composites, that potentially could be applicable are natural composites, nano-engineered composites even hybrid composites, however, the financial concerns as well as the maturity of the manufacturing procedures still favor the typical glass-fiber solution in general. As mentioned, gravitational loads are a design parameter of high importance, which becomes more critical as size and weight of rotor blades increase. Additionally, longer blades deflect more, i.e. the structural stiffness to ensure allowable deflection and tip clearance becomes more significant. Thus, for the material, the stiffness-to-weight ratio is a major design driver as well as the high cycle fatigue behavior of the material interface, given the 20-25 years of designed lifetime which exceeds 100 million load cycles.

1.4 Structural Damage of Wind Turbine Blades

As previously stated, an operational blade is subjected to a complex combination of operational and environmental loads, such as wind pressure, gravitational forces, rain erosion, temperature variations etc. Inevitably, structural damages will accumulate on the blade during its lifetime. Although the inner webs constitute to the main load-carrying sub-components of the blade, it is still the surrounding shells and its surfaces that are most vulnerable and where damages are likely to occur. This is due to the direct exposure of the shells with the surrounding environment. Unaccountable factors, in combination with the operational and environmental loads, such as scratches, impacts and lighting strikes etc. during manufacturing, installation as well as operation, influence damage initiation and growth and can lead to critical, even complete failure of the structure posing fatal economical as well as safety threats.

The main indicators of undesired irregularities and deterioration on rotor blades are discoloration, holes/penetrations and cracks. These can typically be discovered by visual inspection, cf. 1.2, since they occur on the outer surface of the blade. However, as previously emphasized, minor defects such as sub-surface cracks and delamination failures, those in several layers deep, are difficult, if not impossible, to detect visually. To clarify, delamination is a term used widely in material science to describe a failure mode for composites. In laminated composite materials of which turbine blades are comprised, delamination can occur due to the weak adhesive bonding between fibers and the polymer matrix. An impact event from debris-, bird- or lightning strikes can cause delamination and cracks in the resin, greatly reducing the structural health of the composite structure. Even low velocity impacts can cause damage that may propagate into critical failures

[22].

Most manufacturing processes involve separate production of the multimaterial sub-components. The common approach to bond the parts are by means of adhesives and it is known, that adhesive joints represent weak links for the structural integrity. Particularly, the trailing edge joints are notorious for its susceptibility to damage [23]. Empirical sources [20], involving structural testing of turbine blades, indicates that adhesive joints in blades often do not endure their expected lifetime, which consequently leads to considerable expenses because of repair or blade replacement.

1.5 Summary

In present chapter, an outline of the subject of interest has been presented. Firstly, from a wide perspective, the enlarging wind energy sector has been introduced. Secondly, it has been emphasized, that there is a need for a more sophisticated approach to ensure the structural integrity of wind turbines, based on statistical data of related accidents and outdated inspection techniques that lacks a degree of reliability. Thirdly, the specific component of interest has been narrowed down to particularly, the rotor blades. Lastly, the composition, design and conventional materials of the blade component have been elaborated and different types of structural damages have been highlighted, where the attention lays especially on trailing-edge cracks.

From this point, the component of interest has been identified and the project perspective is to facilitate the development of an integrated health monitoring system that potentially will enhance the integrity and reliability of wind turbine blades, leading to an overall decrease in operation-, planning- and maintenance-costs.

Chapter 2

Literature Review

The current development state of the technologies, within the field of structural health monitoring (SHM), is outlined, by reviewing some of the most frequently used methods available for damage identification. Substantive findings, theoretical- as well as methodological contributions from secondary sources of this particular topic will be reviewed. Although damage identification techniques often are application specific, an attempt to review the topic in a general manner is proceeded. Firstly, a brief summary describing the intuition, purpose and benefits of installing a SHM system is presented. Secondly, an overview of different types of techniques is categorized and presented, including a classification system introduced by Rytter, 1993 [24]. Lastly, a list of relevant techniques for wind turbine blades are elaborated with the intention to discard irrelevant methods and select an appropriate approach and focus point for this thesis context.

2.1 Intuition of Structural Health Monitoring

Normally, it is economically beneficial to invest in precautionary arrangements to ascertain the structural integrity of a valuable structure in operation, e.g. the visual inspection approach, cf. 1.2, or a more modern approach involving remote health monitoring equipments. Logically, and as mentioned previously, it is usually less costly to reconstruct and perform maintenance of structures compared to demolition or total replacement.

Structural health monitoring systems can potentially identify damage and provide information to ascertain the condition of a structure so that decisions can be made with regard to the need for remediation. The purpose is to detect, locate and quantify the occurrence, development and severity of structural damages, so that they can be mitigated and vital failures of the structural components can ultimately be prevented. A structure can typically be exposed to a variety of loads, such as wind, gravity, earthquakes, corrosion, rain erosion, thermal gradients etc., a SHM system does not necessarily trace back to, or address, the initiating source of the damage, which likely is a complex combination of more than one load. The SHM system only concerns the actual damage and its significance when it exceeds the preset limitation of a healthy condition. Of course, it is expected that a proper system does not include destructive methods for interrogating the structural integrity, which is why, only non-destructive methods is included in this report.

The potential benefits include enhancing the safety and reliability of the structures with warnings of damage and impending failures, prompting more efficient use of maintenance resources and plan making. An additionally, by monitoring the responses of a structure, information regarding the design current could potentially be provided, so that adjustments can be made resulting in improvements of future structures.

Bridges, satellites, aerospace structures etc. are, among other key structures, potential candidates for SHM applications. A common fact among these structures, as well as for wind turbines, is that they constitute to high-value structures that, in operation, are difficult to access and to perform manual condition assessment of. Automated real-time applications on, for instance, bridges are already in process, see for example the Tamar Bridge in England, [25] and [26].

2.2 Overview of SHM Techniques

The main ability of SHM systems is to identify damages. A slightly modified version of Rytter's (1993) frequently used classification system among SHM literature, to define and categorize the different levels of damage identification, is presented as follows [24]:

Level 1 - **Detection:**	Determine if damage is present in the structure
Level 2 - **Localization:**	Localize the geometric site of the damage
Level 3 - **Assessment:**	Quantify the severity of the damage
Level 4 - **Prognosis:**	Estimate the future progress of damage and predict the remaining service life of the structure

The classification system structurizes the different phases in the process of damage identification. This system is useful when a comparison between different methods is desired. The system is accumulative, which refers to the fact, that level 1 has to be accomplished before one can move on to level 2 and so fourth.

In general, modern methods include sensors and automated reasoning techniques that provide empirical data of the structural health can be inferred from empirical data derived from the structure's response. The types of data that may be used for this purpose are numerous, and the categories of SHM techniques are usually defined by the chosen feature. Several literature, e.g. L. Cartz (1995) [27], T. Uomoto (2001) [28] and B. Raj et al. (2002) [29] have summarized extensive amounts of damage identification techniques, notably chain drags, half-cell potential readings, radiography, ultrasonics, liquid penetrants, magnetic particles, eddy currents, acoustic emissions etc. The equality among these techniques is, that they are non-destructive and their purpose is to detect, locate and characterize defects in different types of structures, referring to the classification system. However, most of these techniques are considered as localized techniques, that in general only are capable of interrogating small areas at a time whereas the region to be inspected must be easy accessible.

From a larger perspective, to interrogate larger areas, global SHM techniques use changes in the overall response of a structure as indicators of damage. These global methods, which also are summarized in several literature, e.g. Schulz et al. (1995) [30], in which semi-static field tests are considered, Jenkins et al. (1997) [31], in which static field tests are considered, and Doebling et al. (1996), in which vibration-based methods are considered. The obvious advantages of these global methods are, that the condition of the entire structure can be assessed at once, and there are less limitations due to inaccessible components. However, the ability of global techniques to locate and quantify the extent of damage is largely unproven to date unless applied to very simple structures.

2.3 SHM Techniques for Wind Turbines

In theory, a wide range of potential techniques can be applied to monitor the health condition of wind turbines. C.C. Ciang et al. (2008) [32] have summarized a list of damage identification techniques for particularly wind turbines. The included methods are namely acoustic emission, thermal aging, ultrasonic, modal-based, fibre optics, laser Doppler vibrometer, electrical resistance, x-radioscopy, strain memory alloy and eddy currents. Among these techniques, the two most recognized methods in active research are notably the acoustic emission method and the modal-based method (also known as vibration-based). Studies have shown, that both of these approaches are capable of detecting and localizing damage processes in wind turbine blades under controlled laboratory tests as well as for operational in-service turbines. For instance, in [33] and [34], where promising results were reported from in-service testings applying acoustic emission techniques to identify damage. The latter approach, namely the vibration-based damage identification technique, is currently advancing in a great amount of studies with promising results. This approach is chosen to be the fundamental basis for the present thesis and its main principles will be elaborated in the following section.

2.4 Vibration-based Damage Identification

The concept of vibration-based damage identification is based on the fact, that modal parameters, notably eigenfrequencies, mode shapes, and modal damping, are functions of the physical properties such as mass, damping, and stiffness. Therefore, changes in the physical properties due to damages, e.g. crack propagation or delamination of bindings, will be detectable by observing the change in modal parameters [32]. The procedure is to prepare and compose a baseline reference model of a healthy configuration focusing on a damage-sensitive vibration feature. By employing this, a structural damage can be detected upon testing of the chosen feature, for instance the mode shapes, exceed or deviate significantly from a certain threshold based on the baseline model. An ideal solution could be to exploit the dynamic responses from a structure induced by operational conditions, however, for wind turbines, studies have shown that the higher frequency responses from a secondary source tend to provide better resolution of damage signatures. For instance in [35], where an actuator has been used to excite dynamic responses upon wind turbine blades.

As previously mentioned, studies have shown, that the vibration-based approach is capable of detecting and localizing damage processes for in-service wind turbines. For instance, the paper by the authors: D. Tcherniak and Lasse L. Moelgaard, [35], demonstrates on a Vestas V27 wind turbine, that trailing edge damages (150 to 450mm openings/artificial introduced damage), were detectable using the vibration response data. More specifically, they used the distinct covariance values obtained upon calculating the covariance matrix of the cross-acceleration data from a number of sensors. In another paper [36], by the authors M. D. Ulriksen, D. Tcherniak and L. Damkilde, damages of the same wind turbine scenario, were confirmed detectable using minor principle components, obtained upon processing and reducing the vibration response data, as damage features. In [37], by the same authors of [35] and [36] except L. L. Moelgaard plus L. M. Hansen, R. J. Johansen and L. Froeyd, demonstrates for same the wind turbine in idle condition, that the trailing edge damages can be localized. Furthermore, [36] reports, that the actual size of the damage can be assessed fairly accurate, hereby promoting an additional level of damage identification, referring to conventional classifications, cf. section 2.2 on page 12.

One common concern mentioned in the papers employing structural health monitoring data from the Vestas V27 wind turbine, which as well is controversial among other SHM applications, is the level of sensitivity that the acquired data have to the varying environmental conditions. This particular issue is chosen to be the main focus point of the present thesis. Further details and potential approaches to ascertain this issue is presented in the following section.

2.5 Damage Detection of Wind Turbines under Varying Environmental Conditions

In contrary to laboratory tests, an in-service wind turbine will expectedly be subjected to varying operational- as well as environmental conditions, which typically will induce non-stationary and quasi-static responses to the structure. These effects have an influence for the ability of conventional vibration-based damage identification schemes to detect damage. Temperature fluctuations, rain variations and different wind speed attitudes tend to have an effect that disrupts the detection scheme by masking important information in the data and prompting false alarms. Temperature is found to be the most dominant factor affecting structural response as it directly affects the stiffness, the structure can for instance become frozen. See for instance [38], where the temperature effects upon modal parameters have been investigated for a bridge.

Theoretically, if a model can predict the value of a monitored feature given the conditions affecting it, the error of the model could be taken account for or even be suitable as a damage-sensitive feature. However, this approach demands a specific and precise understanding of the condition parameters, which also consequently demands, that these parameters have to be monitored i.e. an additional amount of sensing equipments and data. The problem of unavailability of environmental data for wind turbines is a huge restriction for this approach. The economical aspect due to limitations of equipment and data processing procedures will also playa a major role. Another approach could be to monitor the structural responses on a whole-year basis, where the structure have been subjected to the entire range of environmental variations. Logically, this approach requires storage of a large amount of data and an additional drawback is, using a large amount of data to represent a healthy baseline condition may reduce the models sensitivity to damage [39].

A research team from University of Sheffield, UK, has conducted a series of papers regarding structural health monitoring techniques and tests of composite plates plates and bridges (e.g. Tamar Bridge [26]) in both laboratory environments as well in-service environments. This team, consisting of K. Worden and E. J. Cross, among others, have in [40], [41] and cross [42], been focusing on the removal of environmental trends in structural health monitoring data. They are believed to be the first to propose the application of cointegration, originating in the field of econometrics, to SHM data. Another, more popular technique to address the environmental effects, is for instance, using principal component analysis (Also used in [36]), to extract features that are sensitive to damages but less sensitive to the effects of the changing environmental condition [43]. This approach has also been employed by the research team from UK in [40] and [42].

The concept of cointegration, elaborated further in chapter 4 on page 28, involves a cross-test of two ore more non-stationary variables. If a linear combination of the non-stationary series exists to be stationary, the relation between the series will be designated as a cointegration relationship [44]. Traditionally, econometricians employ this cointegration test to determine whether or not a statistical significant relation between two or more variables is present. The purpose could for instance be detrending variables for common trends, or as a tool to establish forecasting predictions. In this engineering context of SHM, the stationary linear combination, found during the cointegration process, could be employed as a feature to detect damage that are insensitive to environmental effects, since this residual will be purged from all common trends [45].

In the field of process engineering, cointegration has been successfully employed to deal with the problem of environmental and operational variability as demonstrated in [45]. The concept of cointegration appears promising and as an applicable technique for the purpose of addressing environmental variations in wind turbine SHM data. Take for instance temperature, which is known to be a dominant factor affecting modal properties of a structure, cf. [38], it is almost completely safe to say, that temperature has a global effect on the entire wind turbine structure. In other words, all monitored data will be subjected to the same temperature and its variations, i.e. be a common trend among the data. This means, that cointegration relationships among the data most likely will exist, and the residual linear combinations can be featured as damage identification parameters. This thesis will pursue to adapt the cointegration technique in order to facilitate the development of a SHM system applicable to wind turbine blades. The decision is made considering, that no other approach, to the authors knowledge, has employed this technique to address environmental effects in structural health monitoring data of particularly wind turbine blades.

Chapter 3

Project Specification

An alternative method, to ascertain the structural integrity of wind turbine blades, is considered to be necessary in the industry of harvesting wind energy. This is due to the conventional antiquated methods consisting of visual inspections, and the increasing volume of turbine installations in more exposed and inaccessible locations. A real-time integrated health monitoring system is potentially able enhance the overall integrity as well as reliability of the wind turbine structure while decreasing labor-, operation-, planning- and maintenance costs.

This project aims to facilitate the development of a structural health monitoring system for wind turbines. The particular component to be focused on is chosen to be wind turbine blade, considering that this candidate is evaluated as the component of highest value and with the highest probability of failure. The theoretical basis, of which the system algorithms are built upon, is a vibration-based damage identification technique. One major issue, prohibiting the development and implementation of a health monitoring system for wind turbine blades, is the confounding influences of environmental effects upon the sensitivity to identify the occurrence of damage. A reliable SHM system must be able to distinguish between changes caused by ambient variations, such as temperature fluctuations, and those caused by damage. This problem of data normalization, which can be ascertained by singling out a damage-sensitive feature from latent environmental influences, is the main focus point to be addressed in this particular thesis context. The technique of cointegration will be employed to establish damage identification features that are in-sensitive to environmental variations. As previously elaborated, cf. section 2.5 on page 15, the stationary linear combination, found during a cointegration process, will be purged from all common trends in the tested data series, i.e. be purged from environmental effects. To the author's knowledge, this specific issue has not been addressed to any applicable extent in current literature, for wind turbines in operation.

The experimental campaign of the V27 wind turbine provides an outstanding opportunity to conduct experimental tests, due to the extraordinary extent of acquired data including, simultaneously, collected meteorological data. Verifications of the proposed methodologies, throughout the report, will be pursued by numerical models with inputs of empirical data collected from this experimental campaign of a full-scale operating wind turbine, which was subjected to trailing edge openings/artificial introduced damage.

3.1 Problem Statement

This present section aims to outline decomposed problem descriptions of the main issue to be addressed: to remove environmental effects in structural health monitoring data.

- **Data preprocessing**
  The acquired empirical data are expected to include noise, delay issues and a conservatively large amount of samples. In this context, preprocessing refers to the necessary operations which are needed to cleanse, align and truncate the data. A visual inspection of the data before preprocessing will help clarifying this particular problem.

- **Extraction of featuring parameters before cointegration**
  The nature of the acquired data can for instance be strains or accelerations, in this case, accelerations. An extraction of the modal properties might be of imperialinterest, if the chosen feature for damage identification is e.g. eigen frequencies or eigenmodes. This can be achieved by use of appropriate software or, of course, numerically by means of modal analysis, which typically include eigenvalue-problems, FRFs and PSDs. This feature selection problem can be solved by trial and error: multiple features can be employed and compared.

- **Damage detection**
  An appropriate method for damage detection has to be chosen. For this purpose, a well-established scheme is considered appropriate. The produced algorithm has to be validated by, for instance, simple numerical simulations using the finite element method or by reproduction of reliable analyses based on the original experimental studies.

- **Reveal the issue due to environmental effects (if possible)**
  In the possession of a well-established damage detection algorithm, one

might be able to reveal the issue of environmental effects upon the sensitivity to identify damage processes.

- **Determine whether or not cointegration relationships exist**
  In order for the residual linear combination to be the final damage-feature in-sensitive to environmental effects, it is imperative, that the data series have cointegration relationships.

- **Comparison of different cointegration techniques**
  Due to the fact that cointegration is a matured technique within the field of econometrics, one might have to compare different types of cointegration techniques, and chose a technique that can be adapted and applied properly to SHM data.

- **Construct features in-sensitive to varying environmental effects and evaluate the results**
  In the completion of the respective points presented above, the results can be evaluated. Questions such as the sensitivity of the residuals to identify damage can be answered. The inherent information and signatures when damage is present in the structure might have been removed in the process. Whether or not cointegration is applicable for the removal of environmental effects can be revealed.

CHAPTER 4

Methodology

The theoretical principles, all of which are applied in the inherent phases of this thesis, are presented in this chapter of methodologies. The essential principles as well as the mathematical methods are explained in a general manner, whereas the actual application will be presented in Chapter 5.

4.1 Modal Analysis

Monitoring the dynamic response of a structure is the primary function of vibration-based SHM systems. Subsequently, potential damage induced changes in the physical properties, i.e. stiffness, mass and damping, can be detected by an appropriate damage identification model. This typically, involves a comparison between the undamaged response data acquired in the healthy state of the structure, and the damaged response data after the occurrence of an eventual damage. The monitored dynamic response can are in general represented by strains or accelerations (e.g. by means of strain-gauges or accelerometers) generated from a source of excitation. In the possession of these response data, a modal analysis can be employed to extract the modal parameters of the structure, i.e. eigenfrequencies mode shapes and modal damping. This process of extraction is conducted by , for instance, solving a generalized eigenvalue problem or by computation of frequency response functions. Further elaboration and analytical examples of modal analysis, for both free-response and forced-response, will be presented in the current section. For a more comprehensive extent of the analysis, the reader is referred to the widely used book for engineering and educational purposes regarding dynamic vibration theory, cf. *"Engineering Vibrations"* [46].

First, a formal introduction of the governing discrete time-invariant equation, widely known as the equation of motion, forming the mathematical foundation:

$$M\ddot{x} + C\dot{x} + Kx = f \tag{4.1}$$

where M,C and K, respectively represent the mass-, damping- and stiffness matrix. $\ddot{x}$, $\dot{x}$ and x are the respective vectors of acceleration, velocity and displacement. The right-hand-side, vector f, is the external force vector.

The system matrices in (4.1) can be derived using, for instance, finite element method, which is based on degrees of freedom at the element nodes, hence, the displacements, velocities and accelerations at any given point in a structure, can be described by an interpolation of the nodal degrees of freedom. For modal analysis, the displacements, velocities and accelerations are expressed by modeshapes, also referred to as eigenmodes, of the structure and. The total number of eigenmodes and eigenfrequencies equal the total number of DOFs and the number of equilibrium equations. Further details about the eigenvalues and the transformation between physical values for each DOF and so-called, modal coordinates, will be elaborated in the following sections.

4.1.1 Eigenvalue Problem of a Free-Response System

In order to present the essence of the fundamental principles in an explanatory manner, the assumptions of time invariance and linearity are considered. For non-linear modal analysis, the reader is referred to [47]. In case of time-invariance, it is assumed that the output of the system is explicitly independent of changes in time. For linearity, it is assumed that the displacements are small, within the region of elasticity, and that the damping matrix can be expressed as a linear combination of the mass- and stiffness matrix. This condition, since both M and K are symmetrical matrices, dictates, that the matrix of C also will be symmetric. However, let it firstly be assumed, that there is no damping, C=0, and no external force, in order to derive the generalized eigenvalue problem, in the condition of a free-response undamped system. The equation for this system can be expressed as:

$$M\ddot{x} + Kx = 0 \tag{4.2}$$

Since, in (4.2), in contrary to (4.1), does not include any damping. The solution to this homogenous differential equation will be oscillatory and yields:

$$x = \Phi cos(\omega t - \varphi) \qquad \vee \qquad \ddot{x} = -\omega^2 \Phi cos(\omega t - \varphi) \tag{4.3}$$

where $cos(\omega t - \varphi)$ is a cosine wave with the angular frequency of ωa and phase φ. By substituting the solutions into (4.3) into (4.2) yields the following:

$$-\omega^2 M\Phi cos(\omega t - \varphi) + \Phi K cos(\omega t - \varphi) = 0 \tag{4.4}$$

With few steps of algebraic manipulation, it is obvious, that the equation constitute to an eigenvalue problem as follows:

$$(K - \lambda M)\,\Phi = 0 \tag{4.5}$$

where λ represents the squared eigenvalues, $\lambda = \omega^2$ and Φ represents the eigenvector.

4.1.2 Modal Decoupling

Upon solving the eigenvalue problem of (4.5), the eigenvectors will form a fully-ranked orthonormal set which can be used to decouple the undamped equations of motion, cf. (4.2). In other words, the modeshapes are orthogonal, which is due to the assumption of linearity, and can be exploited to decouple the equilibrium equations by expressing one equation for each degree of freedom in modal coordinates.

The equation of motion in modal coordinates, i.e. $\ddot{q}, \dot{q}$ and q, is expressed as follows:

$$m\ddot{q} + c\dot{q} + kq = p \tag{4.6}$$

where the modal mass matrix, m, modal damping matrix, c, modal stiffness matrix, k and modal force vector p, can be transformed by use of the original physical system matrices and equal:

$$m = S^T M S \quad \vee \quad c = S^T C S \quad \vee \quad k = S^T K S \quad \vee \quad p = S^T f \tag{4.7}$$

The coordinate transformation procedure:

$$x(t) = [\Phi_1 \quad \Phi_2 \quad ... \quad \Phi_n] \begin{Bmatrix} q_1(t) \\ q_2(t) \\ ... \\ q_n(t) \end{Bmatrix} Sq(t) \tag{4.8}$$

In essence, the modal mass, -damping and -stiffness matrices depend on the eigenmodes:

$$\begin{aligned} m &= [\Phi_1 \quad \Phi_2 \quad ... \quad \Phi_n]^T M [\Phi_1 \quad \Phi_2 \quad ... \quad \Phi_n] \\ c &= [\Phi_1 \quad \Phi_2 \quad ... \quad \Phi_n]^T C [\Phi_1 \quad \Phi_2 \quad ... \quad \Phi_n] \\ k &= [\Phi_1 \quad \Phi_2 \quad ... \quad \Phi_n]^T K [\Phi_1 \quad \Phi_2 \quad ... \quad \Phi_n] \end{aligned} \tag{4.9}$$

Due to orthogonal conditions, the modal mass, -stiffness and -damping matrices becomes diagonal, also known as lumped matrices, i.e.:

$$m = \begin{bmatrix} m_1 & & & \\ & m_2 & & \\ & & ... & \\ & & & m_n \end{bmatrix}, c = \begin{bmatrix} c_1 & & & \\ & c_2 & & \\ & & ... & \\ & & & c_n \end{bmatrix}, k = \begin{bmatrix} k_1 & & & \\ & k_2 & & \\ & & ... & \\ & & & k_n \end{bmatrix} \tag{4.10}$$

The idea of modal decoupling is to reduce the original MDOF system to a number of independent SDOF systems. By doing this, the equilibrium equation for each SDOF system can be solved where contributions are added to the system in order to obtain the MDOF solution. The requirements include, as statet previously, that the system has to be linear. The eigenmodes must be independent and special properties must be fulfilled by the damping matrix C.

4.1.3 Frequency Domain Solution for Forced-Response System

In cases of forced-response, the modal parameters cannot simply be extracted by solving the eigenvalue problem. Forced-response is used in experimental cases, e.g. the experimental study in this thesis cf. chapter 5. The modal parameters can be obtained by exploiting the force induced response and subsequently transform it into frequency domain, in which the parameters can be extracted, [48]. The frequency response function, can be derived by a Laplace transformation of the equation of motion, (4.1) on page 22. Assuming the initial conditions to be zero yields:

$$(Ms^2 + Cs + K)X(s) = F(s) \tag{4.11}$$

Rearranging (4.11) yields:

$$X(s) = (Ms^2 + Cs + K)^{-1}F(s) \tag{4.12}$$

where the matrix inverse, $H(s) = (Ms^2 + Cs + K)^{-1}$, is referred to as the transfer function matrix with complex values of s. The basic formula of a frequency response function can be based on the input $X(s)$ and the output $F(s)$ in the frequency domain, as follows:

$$H(s) = \frac{F(s)}{X(s)} \tag{4.13}$$

The frequency response function is derived by evaluating the transfer function along the imaginary axis, i.e. $s = jw$:

$$H(jw) = (-\omega^2 M + jwC + K)^{-1} \tag{4.14}$$

The physical meaning of the frequency response function is now apparent in (4.14) and the assumption of linearity is not violated since the operation of Laplace is linear.
Since the input, in the experimental study, is in the form of accelerations, each frequency function, $h(jw)$, must be expressed on the kinematic quantities as follows

$$H_{ac}(j\omega) = -\omega^2 H(j\omega) \tag{4.15}$$

4.1.4 Spectral Analysis

Fundamentally a frequency response function is a mathematical representation of the relationship between the input and the output of a system. An approach based on spectral analysis is appropriate to derive the frequency response function, in cases where the system matrices M, C and K are unknown, which is relevant for the experiment in this thesis context. The first step of spectral analysis is to determine the correlation functions of the displacement response, $x(t)$ and the impulse load $f(t)$. This can be determined by following equation of cross-correlation function, C_{xf}, of x and f, [48]:

$$C_x f(\tau) = \lim_{T\to\infty} \frac{1}{2T} \int_{-T}^{T} x(t) f(t+\tau) dt \tag{4.16}$$

where T represents the signal period and τ the time increment. The cross-spectral densities can be derived by Fourier transformation of (4.16), which yields:

$$S_{xf}(\omega) = \frac{1}{2\pi} \int_{-\infty}^{\infty} C(\tau) e^{-j\omega\tau} d\tau \tag{4.17}$$

Now, the frequency response function can be derived by exploiting the spectral density functions. To do this, a selection between different models is necessary, since some are more appropriate than others depending on the expected noise of the respective input and output. Two common models, often referred to as $H1$ and $H2$, are used, respectively, in situations where the output of the system is expected to be noisy (compared to its counterpart, the input) in $H1$, and where the the input is expected to be relatively noisy in $H2$. Other possible models exists but not elaborated in this context. The two transfer function models yields:

$$H1(j\omega) = \frac{S_{xf}(\omega)}{S_{xx}(\omega)} \qquad \vee \qquad H2(j\omega) = \frac{S_{ff}(\omega)}{S_{xf}(\omega)} \tag{4.18}$$

where the S_{xf} is the cross-spectral density function of the input x and output f, as elaborated in (4.17). The S_{xx} and S_{ff} represent the auto-correlated spectral density functions of the respective input and output.
A method, to ascertain the consistency of of $Hj\omega$, is to calculate the coherence function γ^2:

$$\gamma^2 = \frac{|S_{xf}(\omega)|^2}{S_{xx}(\omega)S_{ff}(\omega)} \tag{4.19}$$

Total consistency, i.e. a perfect relationship, is achieved if $\gamma^2 = 1$, in contrary, a complete unrelated relationship between the input- and the output signal when $\gamma^2 = 0$. In a third case, if the squared value is $\gamma^2 \in]0 : 1[$, the coherence function indicates that there exists some undesired external noise in the signals, or a nonlinear relationship between the signals.

4.2 Damage Detection

The imperative foundation of a structural health monitoring system is the scheme to accurately detect the occurrence of a structural damage, cf. the classification system in section 2.2 on page 12. The procedure and the inherent details of a well-established outlier analysis for damage identification are presented The method to detect damage is based on the concept of discordancy from the statistical discipline of outlier analysis [49]. More particularly, the outlier discordancy test for multivariate data used in this context is based on the Mahalanobis squared distance measure, also known as the general squared interpoint distance, and is given by (4.20). Examples of this approach for SHM application are presented in for instance [35], [36] and [42].

$$D^2 = (y - \bar{x})^T S^{-1} (y - \bar{x}) \tag{4.20}$$

where D is the Mahalanobis distance, y is a vector to be tested for discordancy, i.e. the current state potentially constituting to outlying squared distances, $\bar{x}$ is the mean vector of the baseline data, x, and S is the covariance matrix of x. An example on the dimensions is given as follows:

$$x \in \mathbb{R}^{s_l \times n_t} \quad \vee \quad \bar{x} \in \mathbb{R}^{1 \times n_t} \quad \vee \quad y \in \mathbb{R}^{s_l \times n_d} \quad \vee \quad S \in \mathbb{R}^{s_l \times s_l} \tag{4.21}$$

where n_t and n_d refer to the amount of sequences to be included in the respective baseline- and current (potentially damaged) state and s_l refers to the length of the signal. Notice, that the dimensions presented in (4.21) is of general context. The dimensionality might differ depending on the particular applied feature.

In order to label an observation as an outlier, or an inlier, a threshold value must be defined. This value can be exclusively determined using the baseline training data. A straight-forward way to determine the threshold, is to assume, that all data in the training set are in normal healthy condition, yielding that the maximum D^2 distance of this region to be the threshold. However, this solution will neglect possible outliers indicating anomalies in the training set. Depending on whether an inclusive or an exclusive threshold is required, one can make a proper choice.

To demonstrate this outlier analysis based on Mahalanobis metric, an example achieved by means of finite element analysis employing Bernoulli Euler's beam theory can be found in Appendix A on page I, where one of the results is shown in figure 4.1

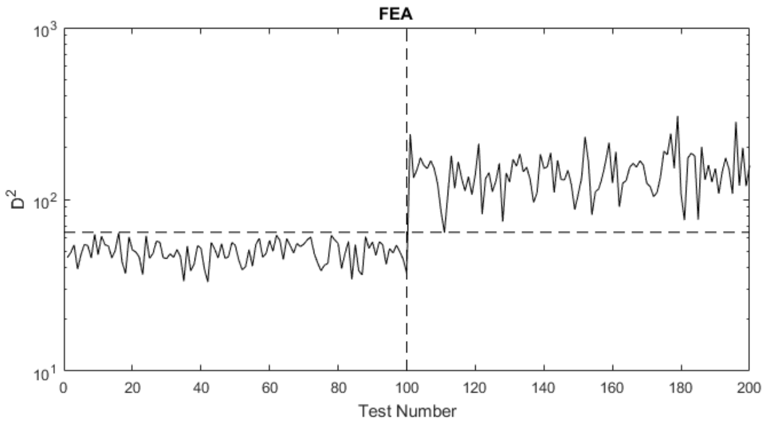

Figure 4.1: Semi-logarithmic plot of outlier analysis based on Mahalanobis squared distance D^2.

The dashed horizontal line indicates the threshold value, ϑ, and the dashed vertical line separates two different structural states. As it can be observed in figure 4.1, the tests from [1 : 100], representing a healthy state of the finite element model, are within the region of inliers whereas the tests from [101 : 200], exceeds the threshold value, i.e. outliers which indicate that some change in the physical properties has been detected. This, "damage", is introduced by reducing Young's modulus, i.e. reducing magnitudes of the parameters in stiffness matrix of the model.

4.3 Cointegration

The theory of cointegration is aimed to be introduced in this current section in a rigorous manner. Firstly, a general introduction of its origination and application in the field of economics, is considered relevant and will be presented. This part is referred as the fundamentals of cointegration, where the background and original purpose will be presented. Examples of where and how cointegration can be applied will also be demonstrated briefly. Secondly, the mathematical and theoretical foundation will be presented, where some of the most common methods within cointegration will be elaborated. These methods will be compared in section 5.5.2 on page 52.

4.3.1 The Fundamentals of Cointegration

Cointegration is an analytical technique in the category of statistical time series analysis and originated in the field of econometrics. The purpose of applying this technique is to test the hypothesis concerning the existence of a statistically significant connection between two or more series of data, i.e. testing for common trends in multivariate time series. The conventional method to address the relationship between non-stationary time series, before the introduction of the cointegrating approach by Clive Granger and Robert Engle in 1987 [50], consisted of using linear regressions, which has been shown to be a dangerous approach that might provide misleading results, [51][44]. For example, regressing on two independent non-stationary series of data, that are not causally related to each other, by means of ordinary least squares, might nonetheless result in high R-squared values, implying a significant correlation, even though it is completely nonsense. This phenomenon, of misleading statistical evidence of a linear relationship between independent non-stationary variables, is known as a spurious regression or as a spurious correlation between the two series of data. By checking upon the existence of a cointegrated combination of two data series, the problem of spurious correlation will be eliminated, and whether or not a genuine relationship between the series is real, can be determined.

Basically, econometricians are often interested in expressing one series according to another and to model their long-run economic relations. Cointegration can be employed to identify common characteristics from which conclusions about their behavior can be drawn. Examples of cointegration relationships in econometrics can for instance be consumption and income, short and long term rates, imports and exports, prices and wages, stock prices and dividends etc.

4.3.2 The Definition of Cointegration

Two or more non-stationary time series are defined as cointegrated if a linear combination of them exists to be stationary. In order to explain this definition formally, a simple case of two time series x_t and y_t is presented in the following equation:

The time series x_t and y_t is considered to be cointegrated if there exists a parameter α such that the residual u_t is stationary:

$$u_t = y_t - \alpha x_t \tag{4.22}$$

One important restriction of the principle, is that all time series must be integrated of the same order. If a non-stationary process x_t becomes stationary after differencing d times, it is said to be integrated of order d, which is denoted as $x_t \sim I(d)$ [45]. By employing a stationary test, the order of integration of a time series is ascertained, which is often the same as testing for a unit root in a time series model since non-stationarity is confirmed if a unit root is present. Popular unit root testing models can for instance be a Phillips-Perron test or a Dickey-Fuller test, of which the last one is demonstrated in the follow section. Subsequently, when the orders of integration been ascertained, the cointegration vector with the most stationary combination can be found. Further elaboration of the inherent steps of cointegration analysis will be described more comprehensively in the upcoming section.

4.3.3 Dickey-Fuller Stationarity Test

The Dickey-Fuller approach tests the null hypothesis of a unit root in an autoregressive (AR) model [52], against the alternative of no present unit root. An AR model, is one that describes the evolution of a time series by a combination of its previous values and a stochastic term. It is a representation of a type of random process, so that it can be used to desrcibe time-varying processes in nature [45]. An AR model of order p is presented as follows:

$$y_t = a_1 y_{t-1} + a_2 y_{t-2} + ... + a_p y_{t-p} + \varepsilon_t \tag{4.23}$$

where y_t is the time series, p is the model order also known as the lagged value, $a_1 ... a_p$ are the coefficients that defines the root characteristics, i.e. the stability and

ε_t is an error term of white noise process with zero mean and constant variance, i.e. a stationary process. To explain a unit root, a simple AR model of first order, AR(1) is considered:

$$y_t = a_1 y_{t-1} + \epsilon_t \tag{4.24}$$

Depending on the value of a_1, three different times serie can be distinguished: $|a_1| < 1$ will yield a stationary process, $a_1 > 1$ will yield a non-stationary process, and $a_1 = 1$ will yield a unit root, which is non-stationary where its first difference will be stationary, since the error term is stationary. This is easily shown, assuming $a_1 = 1$ in (4.24):

$$y_t = y_{t-1} + \epsilon_t \Rightarrow \Delta y_t = \varepsilon_t \tag{4.25}$$

Basically, a time-series can be fitted into an AR model, and then, information on the stationarity of the process is obtained from the parameters defining the characteristic root. This can normally be done by testing a null hypothesis of $a_1 = 1$ using a standard t-test on the parameter. However the leat-squares estimate of the parameter will not be distributed around unity, due to the assumption of non-stationarity and an asymtotic distribution of the t-statistic if $a_1 = 1$ [42]. Hence, Dickey and Fuller have constructed critical values of the t-statistic to be compared [52], known as the DF-statistics, cf. (4.27).

For larger and more complicated set of time series, an augmented version of the Dickey-Fuller Test can be employed. The procedure follows the same premise as the previously elaborated DF-test, however, the model in the ADF-version is more complex and presented as follows [42]:

$$\Delta y_t = \rho y_{-1} + \sum_{j=1}^{p-1} b_j \Delta y_{t-j} + \varepsilon_t \tag{4.26}$$

in which case a unit root will be present if $\rho = 1$. The unit root is here, carried out under the null hypothesis of $\rho = 1$ against the alternative of $\rho < 0$. Futhermore, two optional parameters can be included in (4.26), i.e. vt and μ which respectively represent a deterministic trend and a shift. Once a value for the test-statistic is determined. It can be compared to the relevant critical value of the DF-statistic:

$$DF_t = \frac{\hat{\rho}}{\sigma_\rho} \tag{4.27}$$

where DF_t denotes the DF statistic, σ_ρ the variance of the parameter ρ and the hat, in $\hat{\rho}$ is used to indicate an estimation of the parameter.

Once the degrees of non-stationarity for the series have been ascertained, a stationary residual can be created through combination of those variables integrated to the same order. For this purpose, two popular techniques will be outlined in the following section.

4.3.4 Cointegration Analysis Techniques

In econometrics, the two most common approaches for cointegration analysis are firstly the *Engle-Granger procedure* (1), which is often employed for individual relationships, i.e. when only two process variables are included in the analysis. The second approach is the *Johansen Procedure*(2.), which is a more complex maximum-likehood multivariate estimation procedure that allows for more than one cointegration relationship. Further details of the mathematical procedures are elaborated as follows:

1. The Engle-Granger Procedure

This approach tests the null hypothesis of no cointegration among the time series of interest against the alternative of a cointegration relationship. Engle and Granger recommend a two-step, (i) and (ii), procedure [50]. This approach only concerns individual relationships between, normally, two variables, i.e. the number of variables $n = 2$, in which case the maximum number of cointegrating relationship is one, $r = 1$. It involves a regression of one series upon another and then testing for a unit root.

In order to give an outline of the Engle-Granger procedure and provide the possibility for understanding the inherent processes, a simple bivariate case consisting of x_t and y_t is considered. Followed by the previously elaborated DF/ADF test, the two series can be considered as non-stationary time series integrated of order $I(1)$, i.e. one integration away from being stationary as well as they are unit root processes. In accordance with the definition of cointegration, referring to (4.22), the relationship is considered as cointegrating is there exists a linear combination which is stationary, i.e. the residual sequence is $I(0)$.

(i) The first step is to estimate the static regression, also known as the long-run equilibrium equation [50]:

$$y_t = \alpha_0 + \alpha_1 x_t + u_t \tag{4.28}$$

where the residual u_t is must be a stationary process if the relationship between x_t and y_t is cointegrating. Running an ordinary least squares regression of

(4.28), the residual sequence can be estimated. Again, a hat is used to denote the estimated value, $\hat{u}_t$ and $\hat{\alpha}$, the of linear combination yields as follows:

$$\hat{u}_t = y_t - \hat{\alpha}_0 - \hat{\alpha}_1 x_t \tag{4.29}$$

Now, by testing for a unit root of this residual, in a similar manner such as the DF/ADF test 4.3.3, it can be confirmed whether or not the residual process is stationary. In case the hypothesis of a unit root has been rejected for the residual sequence, one can move on to the second step of the Engle-Granger procedure:

(ii) The second step is to estimate the error correction model (ECM).

The regression parameters estimated in (i) can then be used to construct an ECM which takes the form [41].:

$$\Delta y_t = \rho y_{-1} + \sum_{j=1}^{p-1} b_j \Delta y_{t-j} + \mu + vt + \varepsilon_t \tag{4.30}$$

Theoretically, the error correction model are an approach useful for estimating both short-term and long term effects between two time series. The term error-correction relates to the fact that last-period's deviation from a long-run equilibrium, the error, influences its short-run dynamics. Thus ECMs directly estimate the speed at which a dependent variable returns to equilibrium after a change in other variables [50].

2. The Johansen Procedure

Traditionally, the Johansen Procedure is employed to test multiple numbers of $I(1)$ processes for cointegration. In case the null hypotheses of cointegration relationships, have been failed to be rejected, a number of cointegrating vectors can be established. In contrary to the Engle-Granger procedure, the Johansen procedure provides the ability to determine which cointegrating vectors that create the most stationary linear combination of the analyzed time series. Firstly, this approach utilizes a maximum-likelihood estimation of the parameters of a vector error correction model (VECM) which takes the form [53]:

$$\Delta y_i = \Pi y_{i-1} + \sum_{j=1}^{p-1} \beta_j \Delta y_{i-j} + \phi D(t)) + \varepsilon_i \tag{4.31}$$

where y_i represents a vector including n variables with the subscript i relating to time, Π is the parameter matrix describing the long-run equilibrium. Π can be decomposed into two matrices: $\Pi = AB^T$. Where B is the cointegrating vector of interest in the context og SHM. β_j is a parameter matrix that accounts for the short-run adjustments needed to return the process to equilibrium. The vector $D(t)$ is a term describing a deterministic trend and ε_i represents white noise process as stated previously, but in a vector form in this model. The premise of the Johansen procedure is to use maximum likelihood of observing the correct ε_i to estimate the parameters of Π. The probability density function yields [53]:

$$p(\varepsilon_i) = \frac{1}{\sqrt{(2\pi^n)|\Sigma|}} exp(-\frac{1}{2}\varepsilon_i^T \Sigma^{-1} \varepsilon_i) \tag{4.32}$$

where $|\Sigma|$ is the determinant of the estimated covariance of ε_i. By employing (4.32), the maximum-likelihood parameter estimates will correspond to the parameters that maximize $|\Sigma|$. Upon solving this equation, which eventually involves a generalized eigenvalue problem, the cointegrating vectors will be obtained [54]. A more comprehensive explanation of the inherent steps is to be found in [40]. This approach is also referred to as maximum eigenvalue solution in other literature.

Additionally, after the cointegrating vectors have been found, the Johansen Procedure provides the opportunity to perform a trace-statistic, which determines the solution with most, r cointegration vectors, i.e. most stationarity. This final step in the Johansen Procedure determines whether or not cointegrating relationships are present for the times series. The trace test are presented as follows [40]:

$$\lambda_{trace} = 2logQ(H(r)|H(n)) = \sum_{i=r+1}^{n} log(1 - \lambda_i') \tag{4.33}$$

where Q is the likelihood ratio test which takes the form [40]:

$$Q(H(r)|H(n)) = \frac{|\Sigma(B_{rank=r})|}{|\Sigma(B_{rank=n})|} = \frac{\pounds_{MAX(rank=r)}^{-2/N}}{\pounds_{MAX(rank=n)}^{-2/N}} = \frac{\prod_{i=1}^{r}(\lambda_i' + 1)}{\prod_{i=1}^{n}(\lambda_i' + 1)} \tag{4.34}$$

For econometricians, the key of cointegration procedures is often to establish a significant statistic determining that the variables in consideration are cointegrated or not. From an engineering point of view, the relationship between a set of monitored variables are usually much better understood. The fact that the data are acquired from different spots of the same structural component, and that the surrounding environmental effects have influences on the entire structure, makes the question of cointegration or not less important. The interesting part is the residuals found during the process of testing for cointegration.

The Johansen procedure addresses many of the limitations of the Engle-Granger procedure. It avoids two-step estimators and provides comprehensive testing in the presence of multiple cointegrating relationships. Its maximum likelihood approach incorporates the testing procedure into the process of model estimation, avoiding conditional estimates. At the core of the Johansen method is the relationship between the rank of the impact matrix $\Pi = AB^T$ in (4.31) and the size of its eigenvalues. The eigenvalues depend on the form of the VEC model, and in particular on the composition of its deterministic terms. The method infers the cointegration rank by testing the number of eigenvalues that are statistically different from 0, then conducts model estimation under the rank constraints.

In this thesis context, it is obvious, that the Johansen Procedure is more appropriate than the Engle-Granger procedure, due to the amount of monitored variables, which is greater than two. The Engle-Granger procedure can, in fact, consider more than two variables, however, it will only provide one cointegrating relationship, i.e. one residual and whether or not it is the most stationary linear combination will not be elaborated, whereas the Johansen Procedure provides the ability to find the most cointegrating relationship. The parameter in impact parameter Π, and its rank determine the amount of cointegration relationships. Π must be rank deficient if the error-correction model is to hold true. In case Π has a full rank, the variables in question will not be cointegrated.

Chapter 5

Experimental Study

A research team from Technical University of Denmark (DTU), has during a period of approximately 3.5 months from November 2014 to March 2015, held a measurement campaign on an operating full-scale Vestas V27 wind turbine, with the rated power of 225 kW and rotor diameter of 27 m. This campaign has provided substantial extents of measurement data which provide the opportunity for the team as well as other researchers to conduct tests and analyzes on, so that hypotheses and analytical models, associated to damage identification, can be evaluated experimentally. More comprehensive descriptions of the original campaign details is to be found in [35], written by the authors Dmitri Tcherniak and Lasse L. Moelgaard, and in [36] by Martin D. Ulriksen, Dmitri Tcherniak and Lars Damkilde.

5.1 Experimental Setup

The idea is to identify damage on the blade by monitoring how the vibrations propagate throughout the blade. The vibrations are initiated by hits of an actuator plunger, whereas accelerometers captures the induced vibrations along the blade. During the campaign, five different states were fabricated: A normal (healthy) state, three gradually increased damage states artificially created by trailing edge openings and a repaired state at last.

The health monitoring system, consisting of an electromechanical actuator and an array of accelerometers, was mounted on one, out of the three possible, turbine blades. A sketch illustrating how the monitoring equipments are distributed along the blade is presented in Figure 5.1.

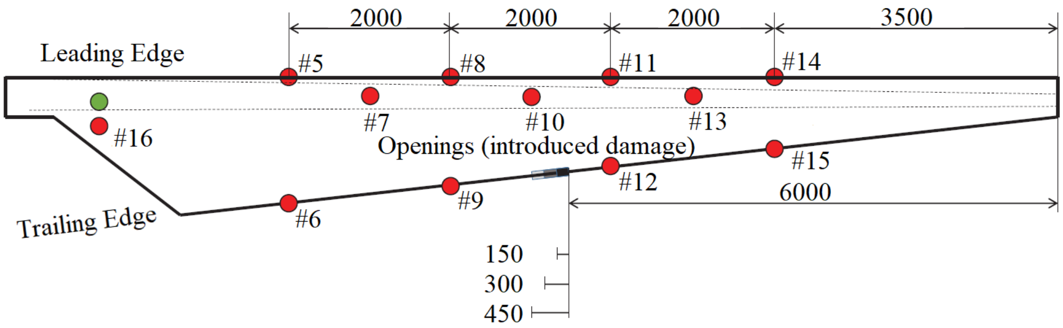

Figure 5.1: Placements of the installed equipment: the actuator (green dot), accelerometers (red dots) with associated enumerations, and the introduced damages (shaded boxes) [55]. All dimensions are in mm.

The significant technical details regarding the instrumentation of the monitoring system are listed in Table 5.1.

Table 5.1: Specifications of the monitoring equipment and instrumentation

Number of Actuators	1
Type of Actuator	Electromechanical, B & K Type 4507B
Number of Accelerometers	12
Type of Accelerometers	Monoaxial piezoelectric, B & K
Nominal Sensitivity #5 to #15	10 mV/ms^{-2} Type 4507B-004
Nominal Sensitivity #16	1 mV/ms^{-2} Type 4507B-001

Notice, that the employed sensors are monoaxial accelerometers and these are mounted on the downwind side of the blade. The measurement direction was aligned normal to the blade, which is also the direction of the force induced by the actuator plunger hit. The sensor of number #16 is actually mounted on the upwind side of the blade and its sensitivity is unique due to the location near the actuator, cf. Figure 5.1. Other means to protect and secure the instrumentation on the turbine blade consist of a waterproof lid, to cover the actuator, mounted with a strap, helicopter tape and silicon to provide smooth surfaces as to adhere the sensors and associated cables to the blade.

The data acquisition system, of which the accelerometers were connected to, consists of Bruel & Kjaer Type 3660- C with two LAN-XI modules, a 12-channel input module Type 3053-B-120 and 4-channel input/output module Type 3160-A-042. Additionally, the pitch angle and rotor azimuth (to ascertain the rotational speed of rotor) were measured, the latter was achieved by two piezoresistive DC accelerometers type 4574-D. This data acquisition system and its electronics were mounted to the inner surface of the spinner and protected inside a waterproof box. The source of power, with the voltage of 24 V, was from the nacelle via a slip ring. The software, Bruel & Kjaer PULSE LabShop, was used to control the system.

5.2 Data Acquisition

As already mentioned, the duration of the measurement campaign was approximately 3.5 months. More accurately, it was 104 days, from 28th of November 2014 to 12th of March 2015. The acquisition software was programmed to acquire 12 sequences of data per hour, i.e. 12 actuator hits per hour. 1 actuator hit corresponds to 16 different signals sampled with 16384 Hz. The duration of 1 sequence was set to 30 seconds: 10 s before the actuator hit and 20 s after the hit. The pause between each sequence, to ensure response independency between the respective sequences, was 4.5 minutes, thus the number of 12 hits per hour and corresponding 12 data sequences per hour. A total number of 24655 actuator hits and corresponding data sets were recorded during the campaign (not 29952 due to the reduced recordings in the period between Christmas and New Year). The turbine was mostly in normal power production regime with the exception of nights, weekends and holidays, in the period of damaged states. It was set to idling when visual surveillance was unavailable, to secure the condition of the turbine when damage was introduced. Although the turbine during that period switched between operating and idling, the monitoring system was still performing and collecting data. Table 5.2 presents the collection of the data sets.

Table 5.2: Acquired data sets from the experiment campaign.

Structural State	**Collected sequences**	**Period of recording**
Normal/healthy	$N_u = 3065$	28-11-14 to 09-12-14
Damaged: 150 mm	$N_{d15} = 1769$	09-12-14 to 15-12-14
Damaged: 300 mm	$N_{d30} = 3407$	15-12-14 to 06-01-15
Damaged: 450 mm	$N_{d45} = 3722$	06-01-15 to 19-01-15
Repaired	$N_{rep} = 12692$	19-01-15 to 12-03-15

The acquired database are stored in hard drives and believed to be physically forwarded around to relevant students and researchers of interest. The data format is compatible with the programming language, Matlab, i.e. ".mat"-files (matrices). References to the data of this state, throughout the rest of the report will be carried out using terms such as original or non-manipulated data, since these data forms the baseline data input. In addition to the empirical data, a few matlab-scipts were included in the hard drive of which the author received. These scripts, presumably created by the authors of [35], namely "FindAccordingly.m" and "Rec.mat", provide the ability for the user to find and return data in accordance with an optional search criteria.

The common signal properties of the acquired data sets, such as sampling frequency and signal length are summarized in Table 5.3

Table 5.3: Common signal properties of the acquired data sets.

No. of signals	**Sampling frequency**	**Time period**	**Signal Length**
$N_s = 16$	$F_S = 16384$ Hz	$T = 30$ s	$S_L = 491520$

For each test sequence, 16 signals were sampled, where 12 of them, [5:16] cf. Figure 5.1, constitute to time-variant acceleration data series from the 12 accelerometers. In addition to the vibration data: rotor data, power production data, yaw angle and a great extent of meteorological data were also included. The latter are collected simultaneously from a weather mast nearby, which consist of wind speed, wind direction, temperature, atmospheric pressure, precipitation etc. For the sake of comprehensiveness, convenience and to create an overview of the available data, all operational wind turbine related- and meteorological data types available are listed in Table 5.4.

Table 5.4: A summary of all the available in the experimental database.

Data type	**Notation**	**Unit**
Acceleration	a	m/s^2
Generator	G	Binary parameter, on/off
Power production	P	kW
Rotor rotation	DC_1 and DC_2	rpm
Rotor azimuth	A_{azi}	°
Yaw angle	A_{yaw}	°
Pitch angle	A_{pitch}	°
Wind speed	W_s	m/s
Wind direction	W_d	°
Temperature	T_C	$°C$
Precipitation	R	m

5.3 Interpretation of Available Data

The empirical data, acquired from the experimental campaign of the Vestas V27 wind turbine, are firstly and most interestingly, the vibrations captured by the sensors, i.e. data in the form of accelerations, m/s^2. These data are the main monitored parameters to preprocess, input and analyzed by means of the damage identification model.Firstly, one sequence of non-manipulated data, including 1 excitation sequence and 11 acceleration sequences from sensor $\#5-\#15$, cf. figure v5.1, is presented in Figure 5.2.

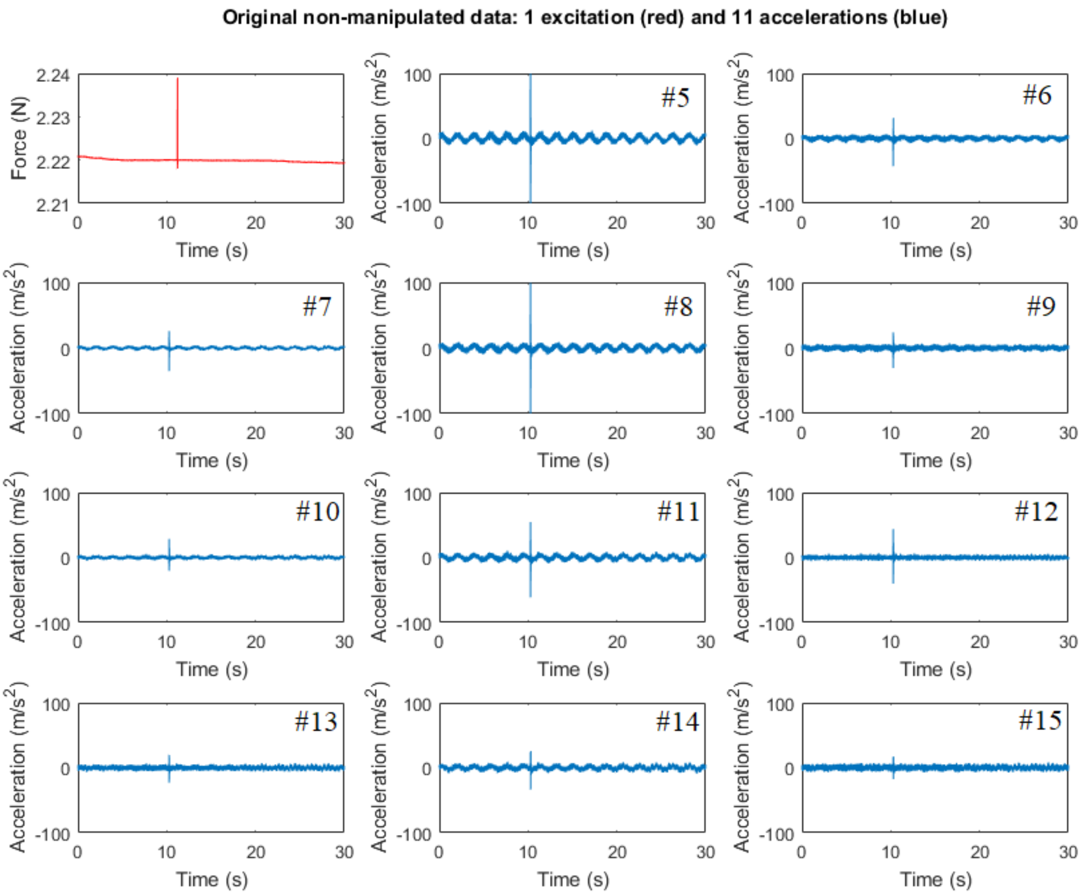

Figure 5.2: Interpretation of available data for each actuator plunger hit. Notice, #16 is excluded. First column: sensors in the middle region (except for the excitation sequence). Second column: sensors along the leading edge. Third column: sensors along the trailing edge. Position from actuator excitation point: Top $\downarrow$ Bottom = Closest $\downarrow$ Farthest.

In order to illustrate the nature the acceleration data, representing the dynamic response of the wind turbine blade, one typical sequence among the acceleration data is displayed in Figure 5.3, and a highlighted region to provide better resolution of the interval of interest, i.e. the period after the peak due to the actuator predominant impulse, is displayed in Figure 5.4.

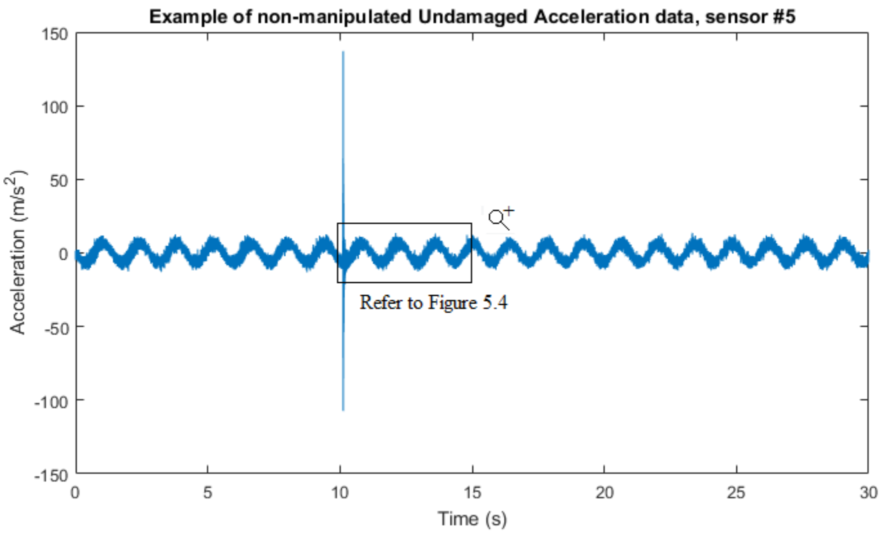

Figure 5.3: A graphical illustration of a randomized acceleration sequence.

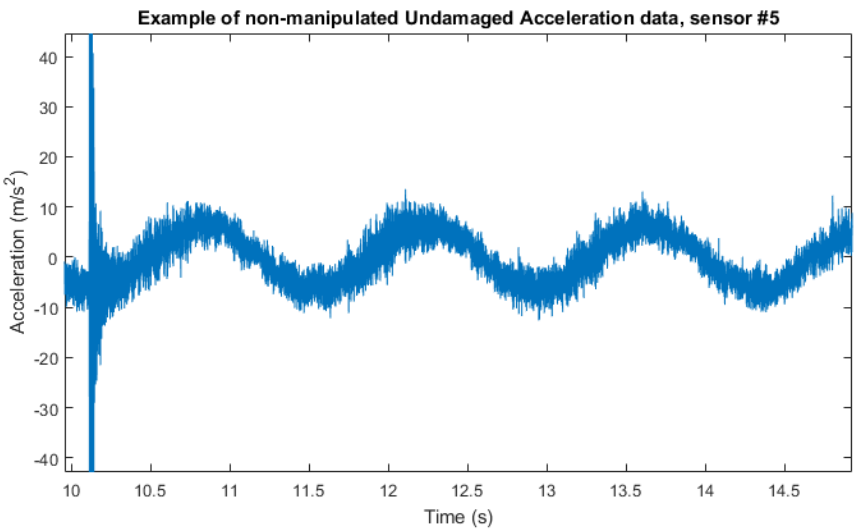

Figure 5.4: A zoomed in graphical illustration of a typical acceleration sequence, highlighting the predominant vibrations induced by the actuator.

The intention of these graphical illustrations in present section is only for illustration purposes of the original data without any processing. Further details regarding preprocessing, postprocessing etc., of the acceleration data will be presented in the upcoming sections.

The main perspective of the thesis is to ascertain the effects of the varying environment of which the wind turbine is subjected to. Fortunately, for this case, a list of meteorological data has been provided. Keep in mind, that these data are assumed to represent the environmental conditions of the Vestas V27 turbine and that possible biases and uncertainties due to the distance between the actual measurement point and the structure itself, are not and will not be considered in this context. These data will be presented in their original form by means of graphical plots of the respective data as a function of sequences. Note, that the acceleration data, presented in figure 5.3 represents 1 single sequence as a function of time, whereas the meterological data plottet in 5.5 represent multiple sequences throughout a longer period. The meteorological sequences of the healthy state sequences and the most damaged state (450mm) sequences are respectively presented in Figure 5.5 and Figure 5.6.

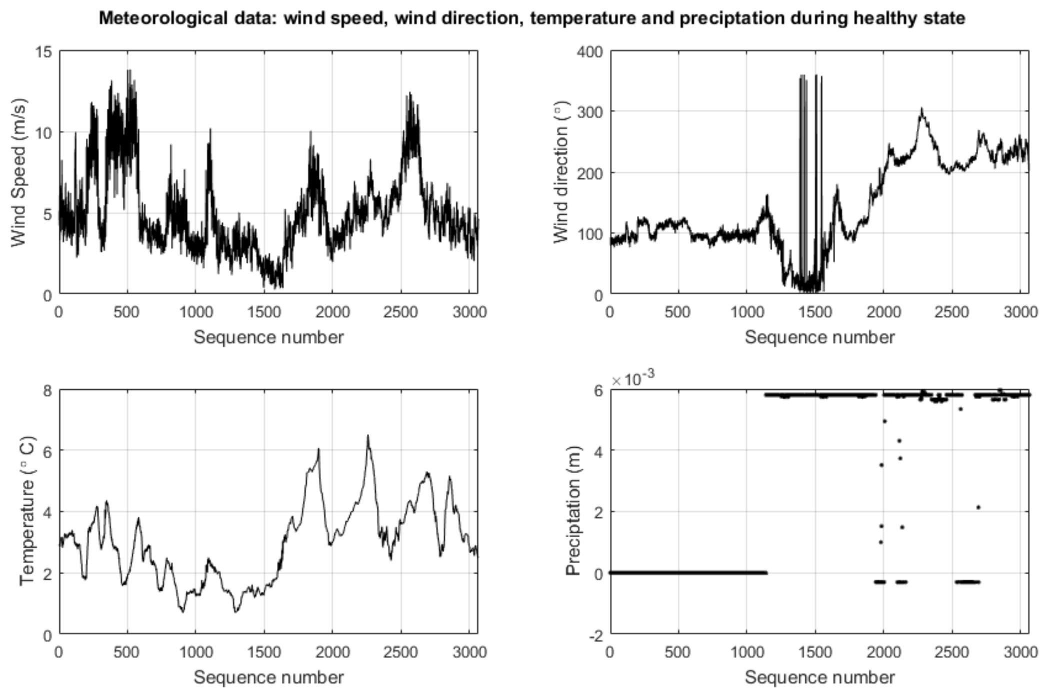

Figure 5.5: Meteorological data capturing during the period from 28-11.14 to 09-12-14, i.e. during the healthy state of the V27 turbine.

Logically, and as observed in Figure 5.5, the Vestas V27 turbine was subjected to different magnitudes of wind speed, temperature fluctuations, varying load conditions due to the wind direction and varying humidity effects caused by precipitation. These environmental properties are evidently influence factors to the structural dynamic behavior of the turbine blade, see for instance, [38], where the temperature effects upon modal parameters have been investigated. In essence, the necessity to account for these environmental effects upon the sensitivity to identify damage, would not be an issue if they were varying consistently, which is why studies in laboratory environments have shown promising results. In order to highlight, that there is difference between the varying condition in the healthy state and the damaged state, the meteorological data collected simultaneously during the latter state, is presented in Figure 5.6

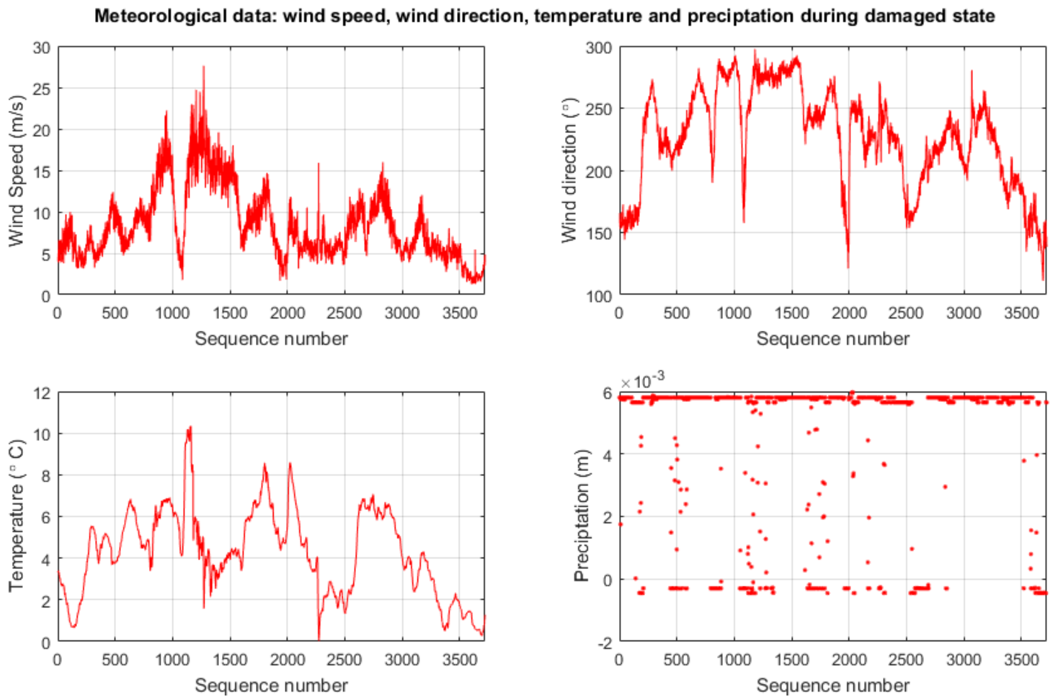

Figure 5.6: Meteorological data capturing during the period from 06-01.15 to 19-01-15, i.e. during the damaged state (450mm) of the V27 turbine.

The wind speed- and temperature variations for both structural states, are summarized in Figure 5.7, in order to make it more convenient for a comparison.

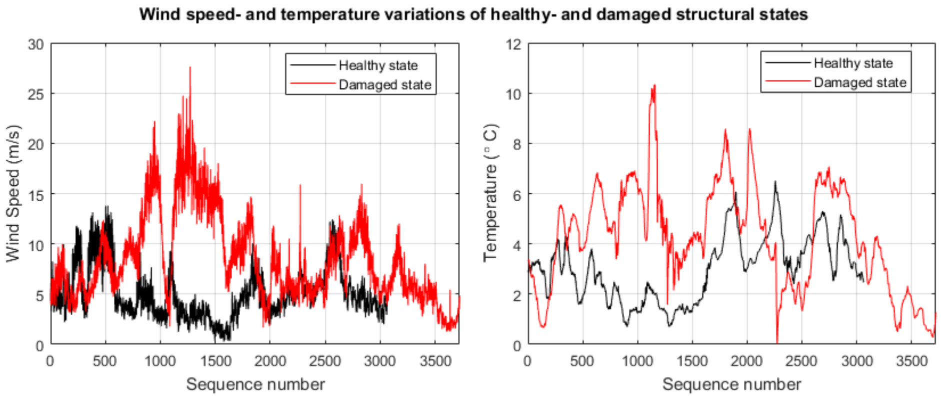

Figure 5.7: Wind speed- and temperature variations for the two respective structural states: Undamaged- (black) and damaged (red) state.

Evidently, the environmental conditions of the two respective structural states are different. This, emphasizes the need for a method to account for these latent influences upon structural health monitoring data. A damage detection test, to emphasize these effects are elaborated further in section 5.5.1 on page 48.

5.4 Data Pre-Processing

This section refers to the signal processing procedures of which the acquired data are subjected to, before implementation and performing numerical tests of cointegration analysis and to identify damage. The intention is to extract damage-sensitive features based on the original acceleration data. Notice, that all data, i.e. in both the healthy and damaged states will be subjected to the similar procedure of preprocessing in order to perform a proper outlier analysis. Due to the similarity in procedure and the large extent of data, only some examples will be presented. To begin with, a visual inspection is performed.

5.4.1 Visual Inspection in Time- and Frequency-domain

In order to evaluate the received data and enhance the first impression of what to be dealt with, a transformation of the signal from time domain into a frequency-domain signal was executed. The reason for this, is that time domain signals only provide information regarding the value of the signal at the given instances. They do not directly interpret information regarding the rate at which the signal is varying. The frequency domain representation of a signal carries information about the signal's intensity and phase at each frequency. To obtain this, a fast Fourier transformation of the original acceleration signal is conducted.

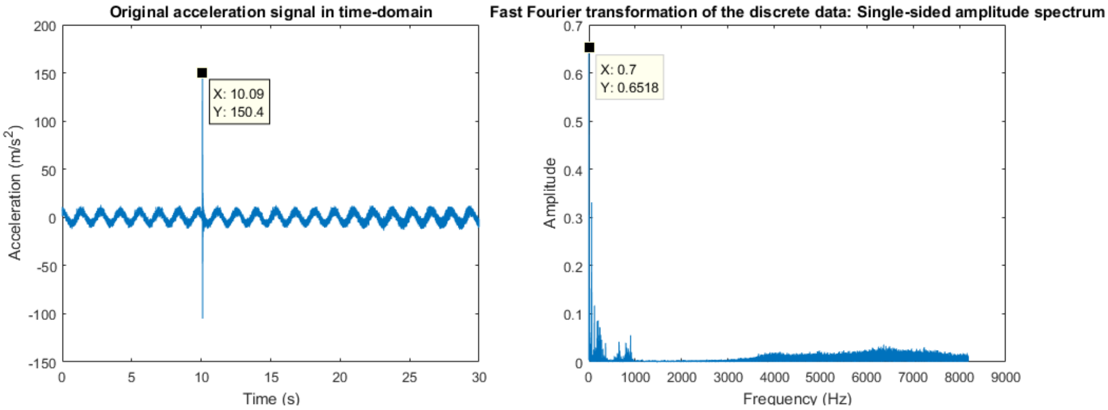

Figure 5.8: Graphical illustrations of an acceleration sequence captured by means of sensor #5, cf. figure 5.1 on page 36, represented in both time-domain (left) and frequency-domain.

Firstly, by looking at the acceleration signal in time-domain, a unique peak at 10.09s can be observed. As described in 5.2 on page 37, the actuator was programmed to release its plunger and induce an impact force on the blade 10s after the beginning of each recording. The observation indicates, that a delay/shift is present and it differs in between the sequences. This is perfectly normal, since the sensors along the blade are located with different distances from the wave propagation starting point. Removing the mean and this alignment issue might have to be taken account for, depending on the specific application approach. The sensor located closest to the actuator, i.e. #16 cf. 5.1 on page 36, can be used for alignment. Furthermore, different orders of periodic oscillatory processes can be recognized in the signal, which confirms, that the turbine is in operation during the data acquisition. Secondly, by looking at the amplitude spectrum in the frequency-domain, it can be observed, that the dominating frequency, i.e. highest peak in amplitude, represents the frequency of the rotor rotation of 0.70 Hz, i.e. 42 rpm. Another high peak in the amplitude spectrum is for instance present at 0.23 Hz, which is a third of the dominating frequency, and most likely due to the fact that the turbine is three-bladed. Furthermore, and as expected, a great amount of external noise is present in both figures. The interesting part of the signal is the actuator-induced vibrations and since it is known, that the applied electromechanical actuator, normally, only excites vibration frequencies around and below 1 kHz, it can be concluded, that the higher frequencies can be discarded. To sum it up, it can be concluded, that the signal has to be aligned properly, truncated to the specific region of interest and filtered to reduce noise and other undesired processes, all of which depending on the application approach.

5.4.2 Frequency Response Function

Frequency response functions can be employed directly as a damage-feature or in order to extract the modal parameters. A matrix of frequency response functions will be estimated based on the input signal as well as the output signal, i.e. the excitation force sequence and acceleration sequences. For this particular estimation purpose, a model using Welch's method has been chosen.

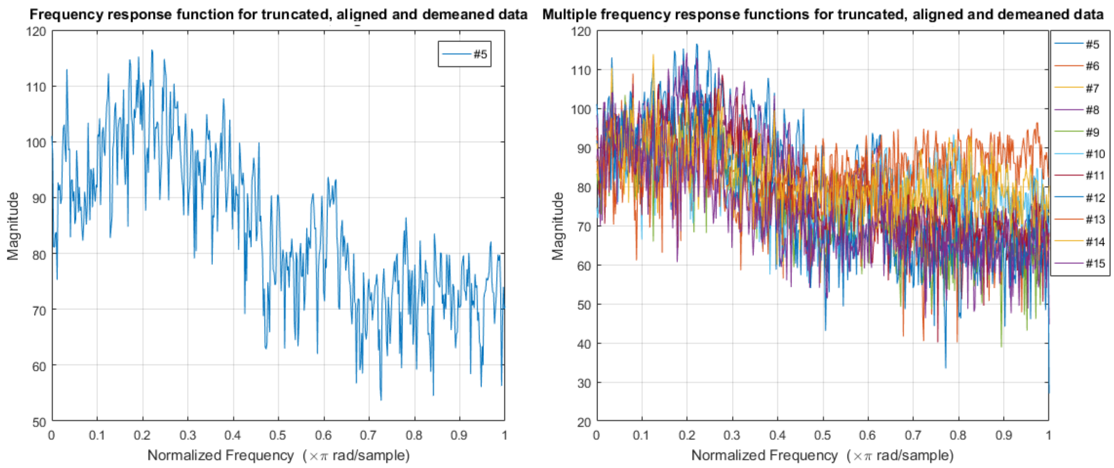

Figure 5.9: Frequency response functions obtained from excitation and acceleration data. To the left, one sequence from sensor #5 has been demonstrated, whereas results from 11 sensors #5 − #15 is shown to the right. The data is obtained during operation condition of the wind turbine with the rotor speed of 42 rpm in this partular illustration.

The length of the original acceleration sequences, which is within the actuator predominant region of the entire signal, is $T = 0.25s$ corresponding to 4097 samples. Notice, that this is the case for the illustrated FRF results in 5.9, alterations of the effective signal length has been used in some of the analyses presented in the upcoming sections. Due to the interest in the high-energy actuator induced frequencies, which is known to be at a medium range around 1 kHz, it has been decided to filter the data from secondary frequencies potentially induced by other sources such as the low-frequencies due to the operation condition as well as high-frequencies with low energy content. The bandpass filter, chosen on basis of a desired bandwidth of 500 Hz and the medium range of 1 kHz yields 1000 Hz ± 250 Hz, i.e. an interval of [750:1250] Hz. For competitiveness, the filtered FRFs, which are conceivably will provide smoother signals, are presented in figure 5.10

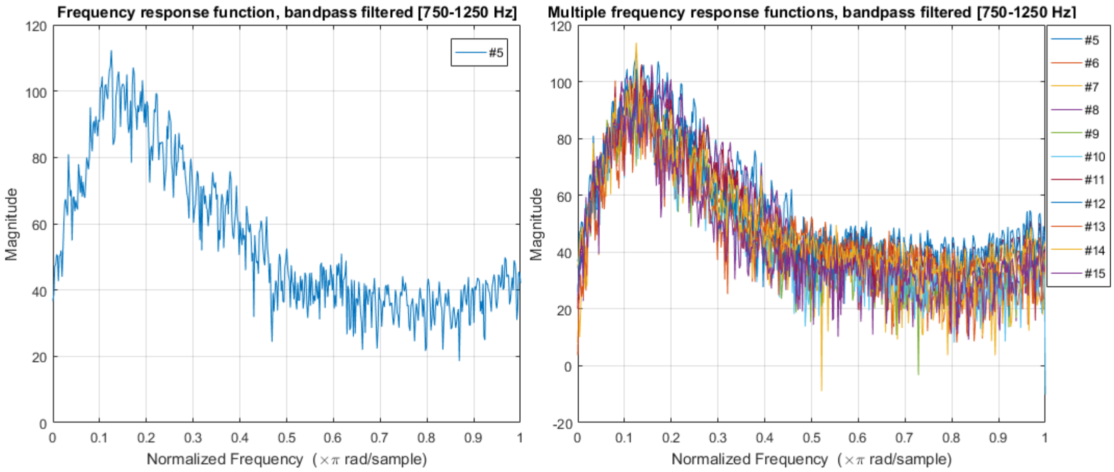

Figure 5.10: Bandpass filtered frequency response functions.

5.4.3 Power Spectral Density

A convenient representation of the strength or energy of a signal can be achieved by estimation of its PSD function. The magnitude of the mean square value of the signal, refers to the power. In for instance [36], principal components of PSDs has been successfully employed for the purpose of damage detection. Figure 5.11 demonstrates PSD functions of the acceleration signal. To demonstrate the energy/power of the induced actuator signal, a PSD outside the actuator region has been estimated as well to create the possibility for a comparison.

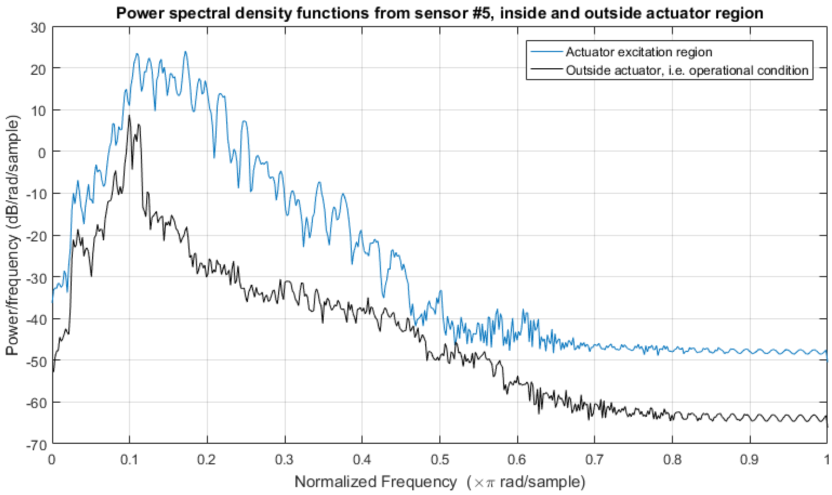

Figure 5.11: Power spectral density functions of two regions within the signal: a region inside the actuator excitation region (blue) and a region outside (black) of the actuators influence, hence the difference in power magnitude.

Obviously, the energy content is higher in the region of actuator excitation and it makes sense to focus on this region.

For competitiveness, an estimation of the power spectral densities of a total of 11 sensors are illustrated in Figure 5.12. Still, the conditions remains in operation with 42 RPM, and the acceleration signal length is $T = 0.25s$ corresponding to 4097 samples.

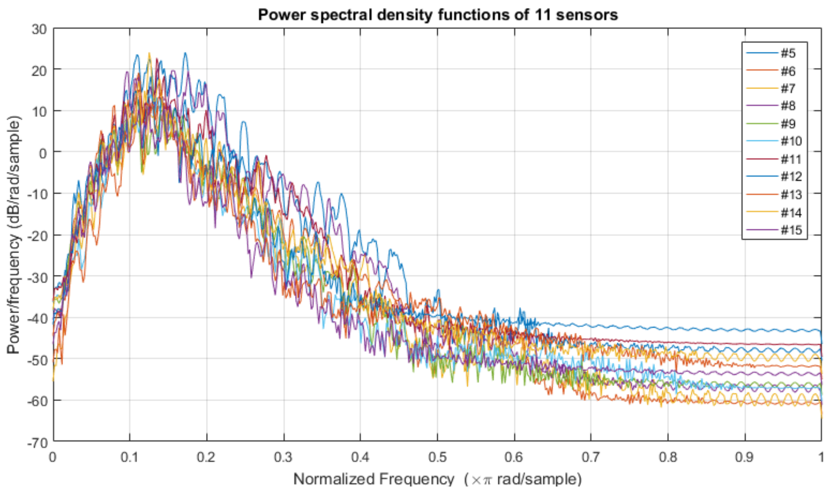

Figure 5.12: Power spectral density functions of a total of 11 sensors, $\#5 - \#15$.

5.4.4 Distinct Covariance Parameters

The authors of the paper [35], demonstrated that distinct values in the covariance matrix (DCM), could be used to detect damage V27 wind turbine. The same premise has been reproduced by the author of this thesis, in order to have a solid and comparable foundation for damage detection. The covariance matrix can simply be calculated and is a square diagonal matrix with the size of $[K \times K]$, where K is the number of sensors. This yields the dimension of $[11 \times 11]$ in this context. Due to the symmetric condition of the matrix, a number of distinct values can be extracted, simply by taking the symmetric half of the matrix including the values in the diagonal. This yields the following a vector of distinct covariance parameters with the size of $K(K+1)/2$. In other words, a vector of the with the length of 66 are constructed in this thesis context, using 11 sensors. The contents in this vector equal covariance values of the variables as well as variance (the diagonal) values of the variables.

5.5 Data Post-Processing

Upon the extraction of a set of features which are considered as secondary representations of the original acquired data, the cointegration analysis can be employed to remove the environmental effects. The original data as well as secondary data, which are in possession after the pre-processing, are in the form of accelerations (A), frequencies obtained from frequency response functions (FRF), power spectral densities (PSD) and distinct covariance parameters (DCM). These parameters have been extracted and stored in matrices, i.e. "-mat"-files, to safe computation time. Before the cointegration analysis is conducted, a demonstration of damage detection analysis is presented, in order to enlighten the issue of environmental effects upon the sensitivity to detect damage processes. For this purpose, the DCM is employed, since the results in [35], indicate that this feature is applicable for damage detection.

5.5.1 Damage Detection using DCM

The damage detection algorithm is based on an outlier analysis based on Mahalanobis metric. For convenience purposes, the formulation presented in section 4.2 on page 26, is recalled as follows, and altered with a subscript D to indicated the particular feature using DCM values:

$$D_D^2 = (y_D - \bar{x_D})^T S_D^{-1} (y_D - \bar{x_D}) \tag{5.1}$$

where D_D^2 is a vector of squared Mahalanobis distances and y_D is a matrix containing the input test parameters potentially outlying. $\bar{x_D}$ and S_D are, respectively, the mean vector and the covariance matrix of the baseline training matrix x_D.

Upon inputting randomized (in healthy state region) DCM values in the baseline matrix x_D, and similarly in y_D (First 100 sequences semi-randomized from healthy state, and last 100 semi-randomized from the damaged state), the results can be obtained. The semi-randomization refers to the fact, that the sequences are sorted based on their condition, but randomized within these criteria. Notice, only the healthy state and the damaged state of 450mm is considered.

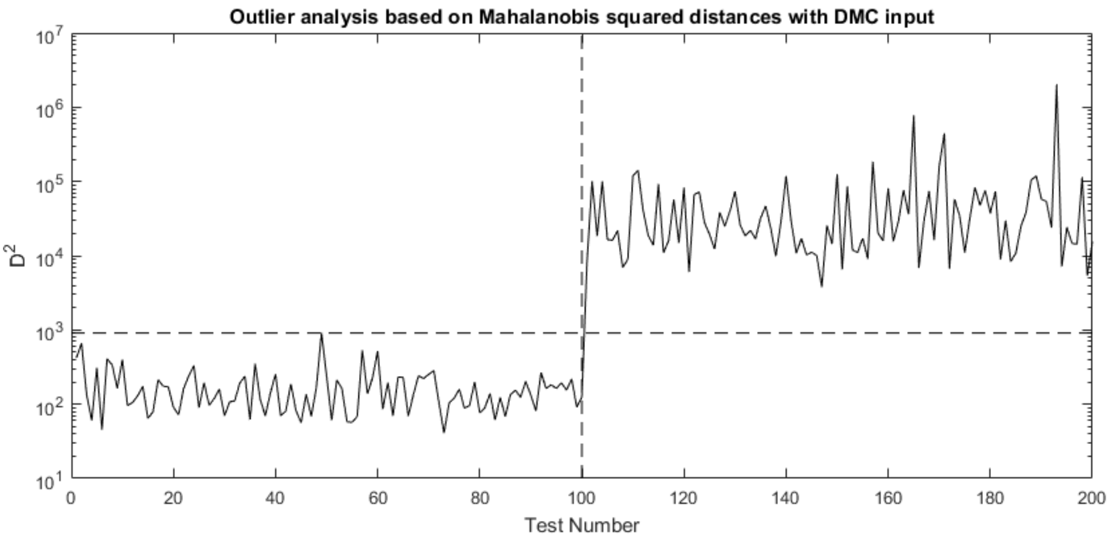

Figure 5.13: Semilogratihmic plot of outlier analysis of Mahalanobis metric for damage detection using DCM values. (reproduction attempt of [35]).

Obviously, the DCM approach is capable of distinguishing a significant difference between the two different states. The test numbers from [1:100] represent the healthy state and [101:200] represent a damaged state. Due to the simultaneously collected meteorological data as well as operation data, it has been possible to single out the sequences and sort them based on their condition. However, if the availability of these data was absent, it would not be possible for the DCM approach to detect damage as robust as presented in figure 5.13. This will be illustrated by a full randomization without any sort of restriction of the input sequences.

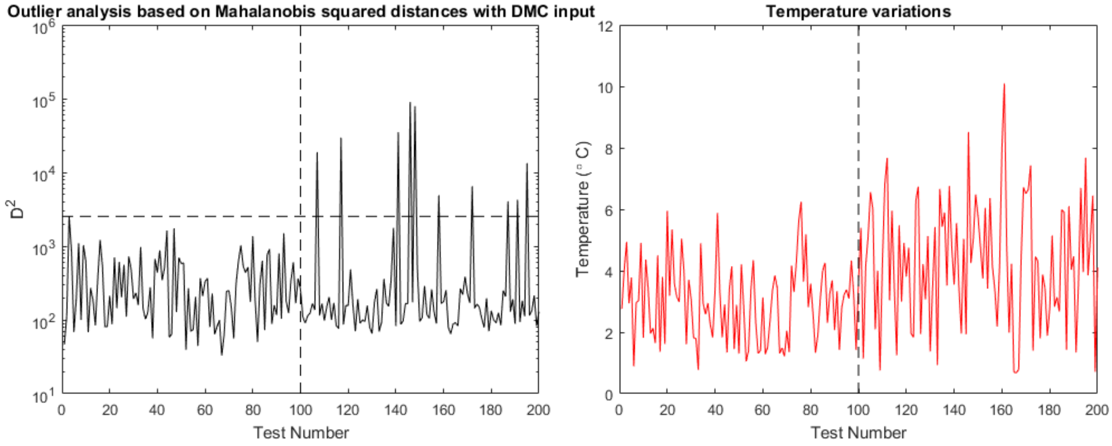

Figure 5.14: Left hand side: Semilogratihmic plot of outlier analysis of Mahalanobis metric for damage detection using DCM values. Right hand side: plot of the respective temperatures for each tested sequence.

In figure 5.14, it can be observed that the DCM approach, in this particular analysis, were unable to detect the damage in the test sequences of [101:200]. No constraints regarding the conditions have been specified in the results of 5.14. The plot of temperature variations highlights, that the temperature during the two states were varying differently and with different magnitudes. This can be an indication of the environmental effects upon the ability to detect damage using DCM. Hence, a method to increase the robustness of the detection algorithm, to be insensitive to environmental effects is desired. This issue is also mentioned in [35].

The reader is referred to the actual algorithm, which can be found in the attached CD in Appendix B on page VII.
Under the file of :"'DETECTION_DCM_REPRODUCTION.m"'.

5.5.2 Cointegration Analysis

As stated in chapter 3 on page 17, the main focus of this particular thesis context is to ascertain the environmental effects on SHM data. It is believed, that in the process of determining the cointegration relationship between the variables of interest, residual sequences will be provided in which all common trends, such as the environmental effects, will be purged.

Test for Stationarity

The first step of cointegration analysis is to address the order of integration of the variables. The definition of cointegration implies, that all variables are restricted to be integrated of same order, preferably the order of I(1), which means that it is one differentiation away from being stationary. Unit root processes are non-stationary processes which will be stationary after one differentiation, meaning that a test for unit root will be sufficient to address this restriction. ADF-tests will be employed for this purpose of unit root testing. The ADF unit root testing approach, tests a null hypothesis of a unit root against the alternative of no unit root.

Recalling the autoregressive model of for an ADF-test, presented in section 4.3.3 on page 29 yields:

$$\Delta y_t = \rho y_{-1} + \sum_{j=1}^{p-1} b_j \Delta y_{t-j} + \varepsilon_t \tag{5.2}$$

where the null hypothesis of a unit root against the alternative of no unit root can be presented formally as follows:

$$\begin{aligned} H_0 &: \rho = 0 \\ H_1 &: \rho < 0 \end{aligned} \tag{5.3}$$

Due to the knowledge regarding the variables, they are expected to be integrated of same order, and expected to be non-stationary processes (at least the accelerations). It is unnecessary to test all data series, since it is obvious, that each type constitute to the same order of integration, however, all parameters is to be tested and be safe, more than one sequence of each type of variable has been tested, where the results yield the same. The results are sumerized in table 5.5.

The results shown in 5.5, indicates that the accelerations and PSDs constitute to unit root processes, since the ADF-test fails to reject the hypothesis of a unit root for these variables. The respective large p_{value} indicates how weak the evidence are against the null hypothesis. Regarding the frequencies of FRF and

Table 5.5: Results of unit root testing based on ADF

	A	DCM	f(FRF)	PSD
H	0	1	1	0
p_{value}	~ 0.300	< 0.003	< 0.003	~ 0.944

DCM values, the ADF-test rejects the null hypothesis of a unit root, i.e. stationary processes, and the small values of p_{value} indicate strong evidence against the null hypothesis. This means, that the frequencies and DCM values will not be suitable for cointegration. The algorithm, providing the results in table 5.5, is provided, referring to Appendix B on page VII, under the filename 'ADFtest.m'.

Demonstration of the Cointegrating Residual based on Accelerations

In order to make an example of a residual sequence, which is the feature expected to be purged from environmental effects, a simple 3-variable case based on presumably, relateable data, in the form of accelerations are used. The acceleration signals have been confirmed as unit root processes, which means that they are suitable for cointegration analysis. The purpose of this is only to demonstrate the trick of employing cointegration analysis, which is why only 3 variables are included. The chosen signals are based on 3 sensors located along the leading edge, namely sensor #5, #8 and #11, cf. figure 5.1 on page 36. The length of the signals are for illustrative purposes chosen to be 5s, starting from the actuator excitation region.

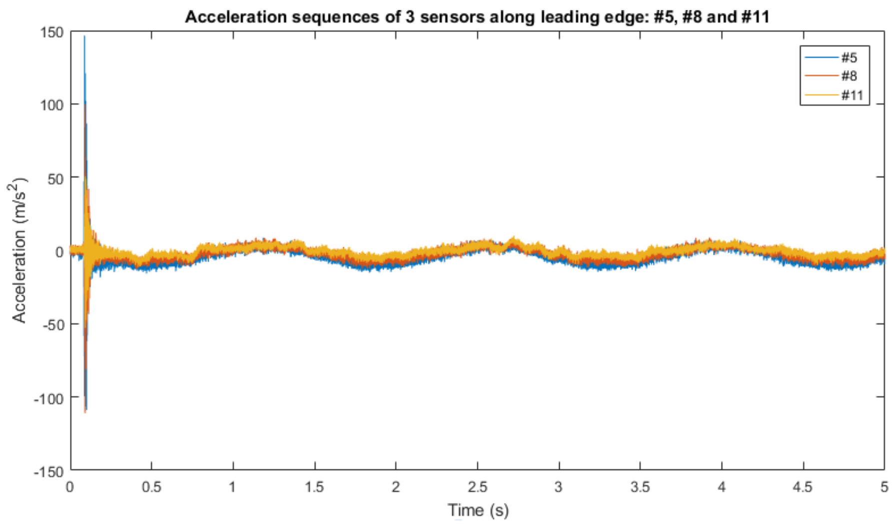

Figure 5.15: Simple plot of 3 acceleration signals located along the leading edge og the wind turbine blade.

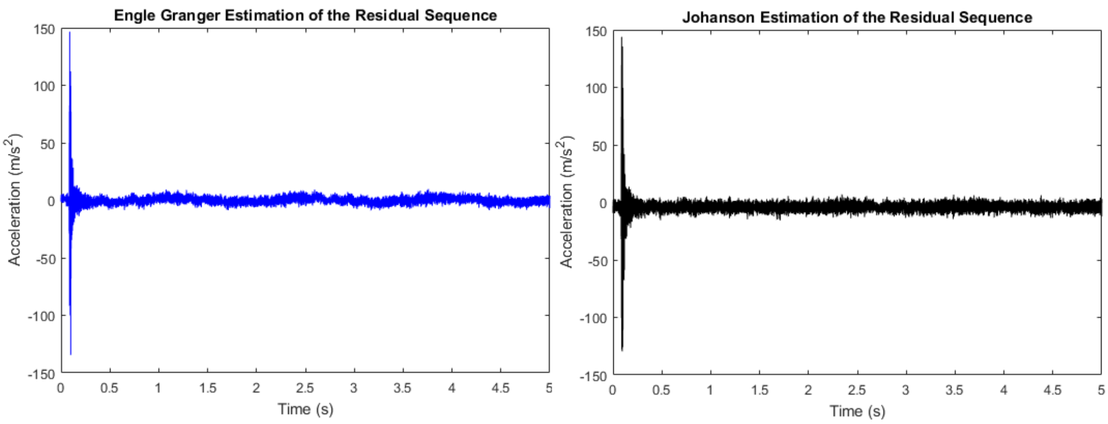

Figure 5.16: The corresponding residual sequence found in the process of cointegration analysis. The result from Engle-Granger (blue) to the left and the result from Johansen (black) to the right.

The residual sequence, which is a linear combination of the acceleration signals, is a stationary process in contrary to its counterparts: the non-stationary acceleration sequences. An additional example, of the same three sequences with a shorter signal length is presented as well, in order to be able to examine the sequences in higher resolution.

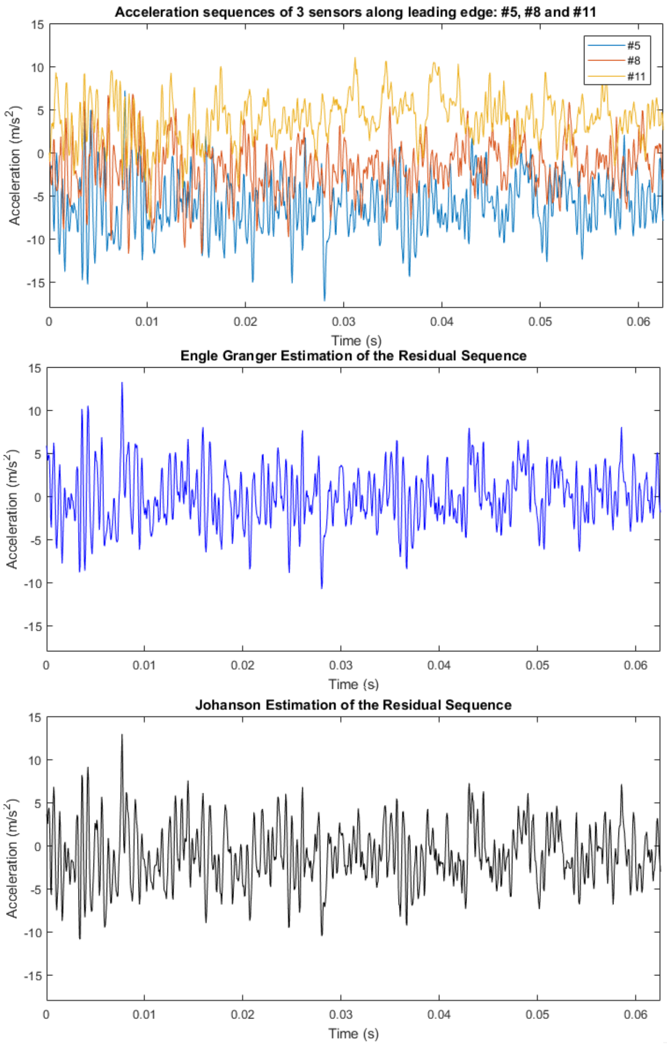

Figure 5.17: Demonstration of the residual sequence based on 3 acceleration sequences. The top plot, middle plot and bottom plot, respectively, represent the acceleration signals, the corresponding residual sequence obtained by Engle-Granger approach and the residual sequence obtained by Johansen approach.

The length of the signals in figure 5.17 are $T = 1/16s$, which provides must higher resolution for further inspection of the residual sequence. This residual sequence is purged from common trends among the acceleration data, i.e. regardless of the environmental condition, the residual will become stationary and constitute to a feature which can be used for damage detection, that are in-sensitive to environmental effects. The reader is referred to the actual algorithm, providing the results in figure 5.16 and 5.17, which can be found in the attached CD in

Appendix B on page VII. Under the file of :'RESIDUAL_PLOT_DEMO.m'.

This procedure of estimating the residual linear combination, will be performed including all sensors in the final analysis, i.e. 11 time series with the possibility of 10 cointegration relationships. The Engle-Granger approach only provides the possibility of estimating 1 cointegration relationship, i.e. one residual sequence, and it depends how the variables are positioned upon estimation. The Johansen procedure provides the ability to estimate the most stationary residual, which is obviously more appropriate, and the reason why this particular method will be used in the upcoming sections.

5.6 Demonstration of Damage Detection Results based on Residual Sequences

The results presented in this section, are based on a discordancy tests between two structural states of the V27 wind turbine. Since the particular perspective of this thesis is to ascertain the environmental effects, only the healthy state and the damaged state of 450 mm trailingedge openings will be considered. The capability regarding whether or not the sensitivity of the damage identification method to detect relatively small scale damages is already considered in [35] and [36]. Temperature variations have been elaborated as the environmental parameter with the highest effects upon structural health monitoring data, which is why this particular parameter is included in the following presentation of the results.

Firstly, results obtained by acceleration residuals will be presented, for this purpose 3 separate analysis, representing 3 attempts on detecting damage is presented in figure 5.18. Note, that the sequences is randomized among the 3065 possibilities for the healthy state at 3722 possibilities for the damaged state. In those particular results, no restriction critiria has been defined, since the purpose is to develop features which robust regardless of its condition.

Secondly, the results obtained by PSD residuals will be presented, cf. 5.19. In a similar manner as previously stated, no search criteria restriction and randomized among the available sequences within the structural state of healthy as well as damaged (450 mm).

The reader is referred to the actual algorithms, which can be found in the attached CD in Appendix B on page VII. Under the files of:
'COINTEGRATION_DETECTION_ACC.m' and
'COINTEGRATION_DETECTION_PSD.m'.

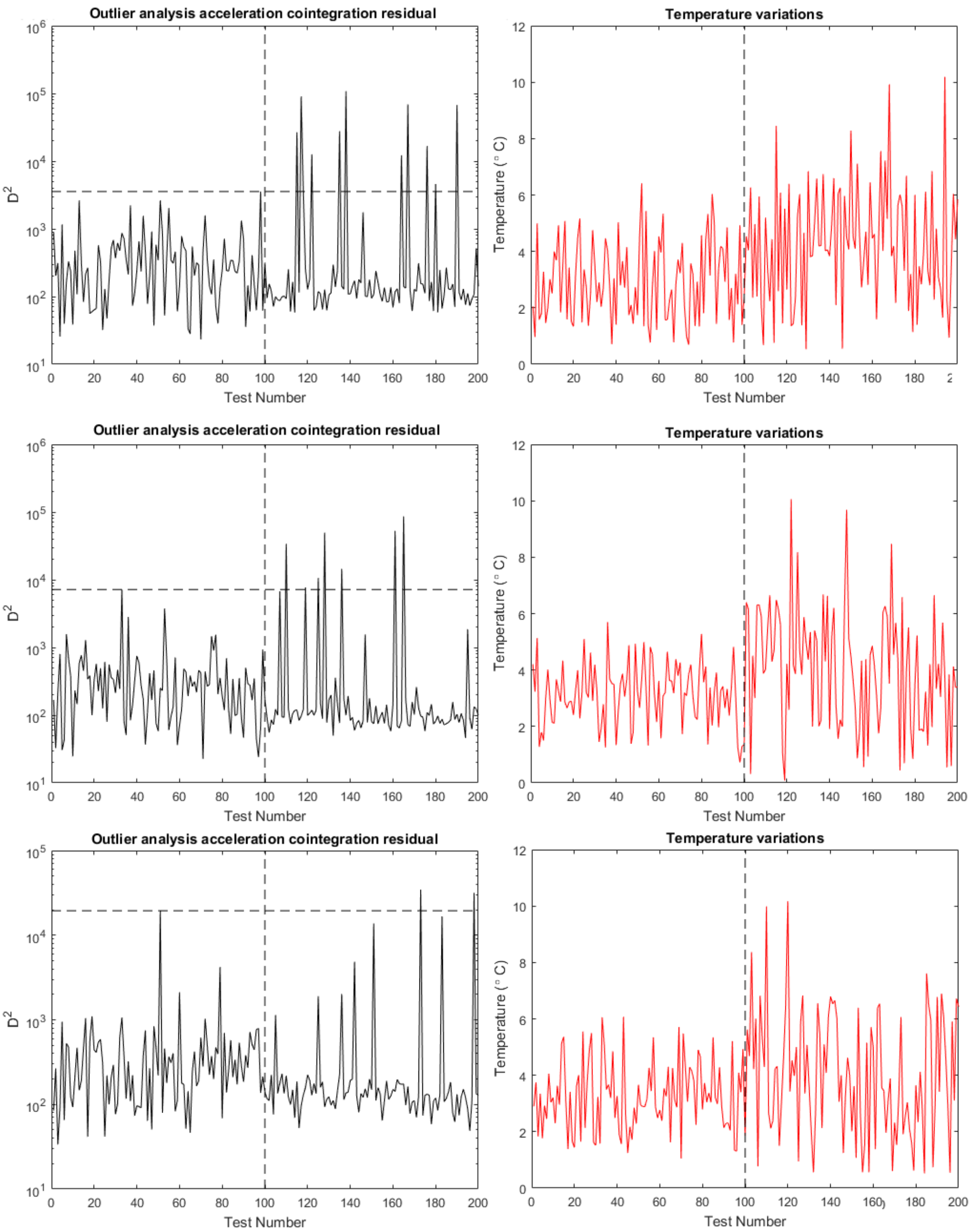

Figure 5.18: Semilogarithmic plot result of 3 separate attempts to detect damage based on outlier analysis using Mahalanobis, where the featured input is residuals of cointegrated acceleration data.

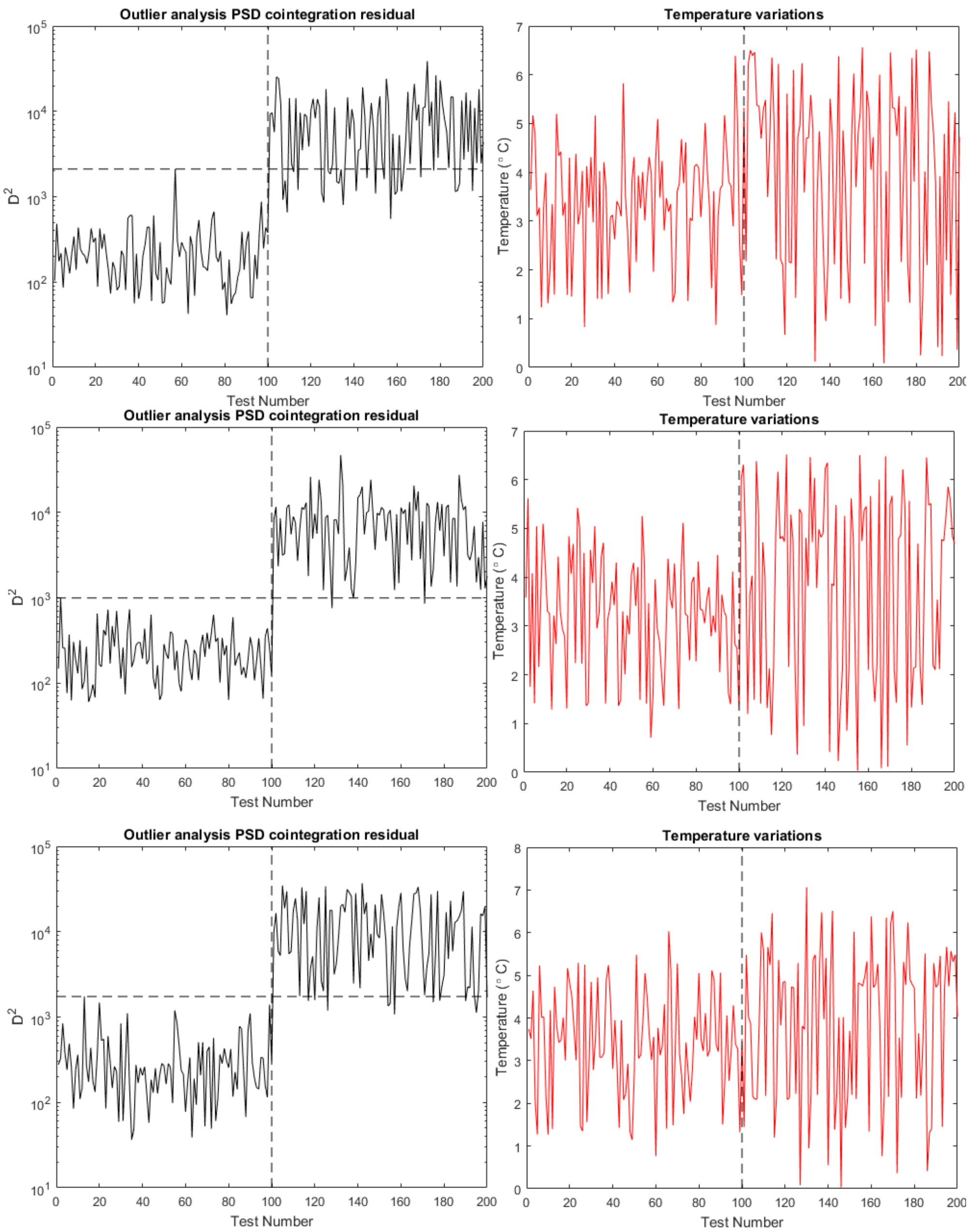

Figure 5.19: Semilogarithmic plot result of 3 separate attempts to detect damage based on outlier analysis using Mahalanobis, where the featured input is residuals of cointegrated PSDs.

Chapter 6

Conclusion

As stated in the chapter of Project Specification, cf. chapter 3 on page 17, the present project aims to facilitate the development of a reliable health monitoring system for wind turbines. One imperative requirement, before SHM systems can be implemented in practical, is the ability to detect damage regardless of the environmental condition that the turbine is subjected to. It is well-known that, for instance, temperature variations have considerable effects on the modal parameters of a structure. This is a concern that to be addressed, since conventional methods to identify damage are based on monitoring changes in the modal parameters.

In order to address this particular issue, a statistical analysis technique from the field of econometrics have been employed, namely cointegration. The principles of this concept is that two (or more) time series, are considered as cointegrated, if a linear combination of them is found to be stationary. Basically, if such combination exists, the two time series must have some level of common behavior and tendencies. Upon the process of establishing cointegrating relationships, this residual linear combination will be found and will be purged from all common trends. Usually, From an engineering point of view, structural response data, which are used for damage identification, are more tangible and more predictable since they represent the behavior of physical objects. Due to the fact, that monitored data are, at least for this case, obtained from the same structure, it can be presumed, that they have common trends, since they are subjected to the same environmental condition. This project has, based on this assumption, utilized the residual linear combinations obtained during the process of cointegration analysis, to be featured as damage identification parameters, where environmental effects have been removed. The capability of cointegration residuals to be featured as damage identification parameters have been explored based on inputs of experimental data collected from a full-scale operating Vestas V27 wind turbine.

A recall of the inherent processes is summarized as follows: Firstly, the empirical data, obtained from the experimental campaign of a Vestas V27 wind turbine, were pre-processed. In this phase, the data were subjected to truncation, alignment and bandpass filtering, and subsequently, the frequencies upon estimating frequency response functions, power spectral density functions and distinct covariance parameters, were, respectively, extracted from the original data sets. Secondly (post-processing), the extracted parameters were subjected to a unit root test, based on an augmented Dickey-Fuller test, where the results indicated, that the parameters suitable for cointegration analysis were notably: the original acceleration data and the power spectral density functions. A simple case with 3 acceleration signals was then demonstrated to highlight the results of residual sequences found during the process of cointegrating. These residual sequences, which is stationary linear combinations of the input data (for instance accelerations and PSDs) are expected to be purged from all common trends. The same premise, as demonstrated for the simple case of acceleration signals, were then numerically applied for both the acceleration data and the data of PSDs, i.e. two parameters were subjected to cointegration analysis. For both types, the analysis provided a number between 1 to 10 residual sequences for each actuator excitation, due to the employment of 11 sensors. The different ranks of the resulting impact matrices Π, indicates the amount of cointegrating relationships, which was found to be inconsistent. This is expected, since the sensors closer to one another tend to have higher probability for common trends, i.e. the distance between the sensors will play a role on whether or not they are cointegrating. The majority of the sequences had approximately 5 cointegration relationships. This information is gained through experience upon developing and estimating the residual linear combinations.

Upon the possession of the residual linear combinations of respectively accelerations and PSDs, damage detection analyses were then conducted based on outlier analyses of Mahalanobis squared distances. By observing the results, it can firstly be concluded that the residuals of acceleration data can not be used to identify damage. This is on some level expected in advance, since it is mainly the modal parameters that constitute as damage-features with signatures of damage. The features such as frequencies and distinct covariance values, were, in fact, also attempted to be implemented as inputs in numerical algorithm, however, the results indicated that these parameters were unsuitable for cointegration analysis, and therefore discarded. Lastly, regarding the most successful parameter among the extracted features, the PSD residuals: According to the results presented in 5.6 on page 55, one can get the impression, that this feature is robust against environmental variations and is capable of detecting damage.

Bibliography

[1] European Commission. *Energy 2020: A Strategy for Competitive, Sustainable and Secure Energy.* Directorate-Genaral for Energy. Luxembourg, 2011.

[2] MHI Vestas Offshore Wind. *Leading Edge technology: Turbine and Innovations.* 2017, (Accessed 12-02-2018). URL: `http://www.mhivestasoffshore.com/innovations/`.

[3] Wind Power Monthly. *Ten of the Biggest Turbines.* 2017, (Accessed 12-02-2018). URL: `https://www.windpowermonthly.com/10-biggest-turbines/`.

[4] MHI Vestas Offshore Wind. *V164-8.0 MW Breaks World Record for Wind Energy Production.* Matt Whitby Press and Communication Officer, 2014, (Accessed 12-02-2018). URL: `http://www.mhivestasoffshore.com/v164-8-0-mw-breaks-world-record-for-wind-energy-production/`.

[5] Science Alert: David Nield. *This Monster Wind Turbine Just Set a New Record For Energy Output.* 2017, (14-02-2018). URL: `https://www.sciencealert.com/monster/wind-turbine-sets-a-new-record-for-energy-output`.

[6] GE Renewable Energy. *Haliade-X Offshore Wind Turbine Platform.* Halide-X 12 MW 107, 2018, (Accessed 14-02-2018). URL: `https://www.ge.com/renewableenergy/wind-energy/turbines/haliade-x-offshore-turbine`.

[7] Better World Solutions. *Lockheed Martin Designed Giant 50 MW Wind Turbine.* Segmented Ultralight Morphling Rotor, 2017, (Accessed 14-02-2018). URL: `https://www.betterworldsolutions.eu/lockheed-martin-designed-giant-wind-turbine-of-50-mw/`.

[8] Sandia National Laboratories. *Sandia Labs News Releases: Enormous Blades Could Lead to more Offshore Energy in U.S.* Segmented Ultralight Morphling Rotor, 2016, (Accessed 14-02-2018). URL: https://share-ng.sandia.gov/news/resources/news_releases/big_blades/#.WwRkxUiFOUk.

[9] Fast Company: Ben Schiller. *Inspired By Palm Trees, These Wind Turbines Bend And Fold Away During Hurricanes.* Segmented Ultralight Morphling Rotor, 2016, (Accessed 14-02-2018). URL: https://www.fastcompany.com/3056375/inspired/by/palm/trees/these-wind-turbines-bend-and-fold-away-during-hurricanes.

[10] Caithness Windfarm Information Forum. *Accident Statistics.* 31-03-2018, (Accessed 01-04-2018). URL: http://www.caithnesswindfarms.co.uk.

[11] WindAction. *Wind turbine collapses for no obvious reason.* 24-05-2017, (24-02-2018). URL: http://www.windaction.org/posts/46755-wind-turbine-collapses-for-no-obvious-reason#.WbI5jMgjGUl.

[12] Kiowa Country Signal. *Wind turbine collapses for no obvious reason.* 23-05-2017, (Accessed 24-02-2018). URL: http://www.kiowacountysignal.com/news/20170523/wind-turbine-collapses-for-no-obvious-reason.

[13] Caithness Windfarm Information Forum. *Wind Turbine Accident And Incident Compilation.* 31-03-2018, (Accessed 01-04-2018). URL: http://www.caithnesswindfarms.co.uk/fullaccidents.pdf.

[14] GCube: Provider of renewable energy insurance services. *Top 5 US Wind Energy Insurance Claims Report.* 13-09-2017, (Accessed 24-02-2018). URL: https://www.lmwindpower.com/en/products-and-services/service-and-maintenance.

[15] Windpower Monthly. *Annual blade failures estimated at around 3.800.* 14-05-2015, (Accessed 26-02-2018).
URL: http://www.windpowermonthly.com/article/1347145/annual-blade-failures-estimated-around-3800#disqus_thread.

[16] Faisal Khan M. Mohsin Khan, M. Tariq Iqbal. *Reliability and condition monitoring of a wind turbine.* Memorial University of Newfoundland, St. Johns, Canada, Canadian Conference on May 2005. pp. 1978-1981.
ISBN: 0-7803-8885-2.

[17] LM Wind Power. *Service and maintenance.* 06-08-2013, (Accessed 24-02-2018). URL: http://www.gcube-insurance.com/press/gcube-top-5-us-wind-energy-insurance-claims-report/.

[18] L. Mishnaevsky Jr., K. Branner, H. Noergaard Petersen, J. Beauson, M. McGugan, and B. F. Sorensen. *Materials for Wind Turbine Blades: An Overview.* Department of Wind Energy, Technical University of Denmark. 4000 Roskilde, Denmark, 9 November 2017.

[19] B. F. Soerensen. *Materials and Structures for Wind Turbine Rotor Blades - an Overview.* Materials Research Department, Risoe National Laboratory. 4000 Roskilde, Denmark, 2017.

[20] S. Ataya and M.Z. Ahmed. *Damages of Wind Turbine Blade Trailing Edge: Forms, Location, and Root Causes.* Engineering Failure Analysis. Vol. 35, pp. 480-488, December 2013.

[21] C. Granger and P. Newbold. *Cost Study for Large Wind Turbine Blades: WindPACT Blade System Design Studies.* Sandia Corporation, a Lockheed Martin Company, 2003.

[22] M. O. W. Richardson and M. J. Wisheart. *Review of Low-velocity Impact Properties of Composite Materials.* Composites Part A: Applied Science and Manufacturing. Vol. 27, No. 12, pp. 1123-1131, 1996.

[23] P. U. Haselbach, M. A. Eder, and F. Belloni. *A Comprehensive Investigation of Trailing Edge Damage in a Wind Turbine Rotor Blade.* John Wiley & Sons, Ltd. Wind Energy, Volume 19, pp. 1871-1888, October 2016.

[24] A. Rytter and P. H. Kirkegaard. *Vibration Based Damage Assessment of Civil Engineering Structures Using Neural Networks.* Aalborg University, Denmark. Vol. 58, No. 1, pp. 165-193, 1993.

[25] N. Battista, R. Westgate, K. Y. Kooa, and J. Brownjohn. *Wireless Monitoring of the Longitudinal Displacement of the Tamar Suspension Bridge Deck under Changing Environmental Conditions.* Department of Civil & Structural Engineering. University of Sheffield, UK, 2011.

[26] K. Y. Koo, J. M. W. Brownjohn, D. I. List, and R. Cole. *Structural Health Monitoring of the Tamar Suspension Bridge.* Department of Civil & Structural Engineering. University of Sheffield, UK, 2012.

[27] L. Cartz. *Nondestructive Testing.* Marquette University, College of Engineering, Milwaukee WI USA. The Materials Information Society., 1995.

[28] T. Uomoto. *Non-Destructive Testing in Civil Engineering 2000.* Elsevier Science. ISBN: 9780080545356, 1995.

[29] B. Raj, T. Jayakumar, and M. Thavasimuthu. *Practical Non-destructive Testing.* Woodhead Publishing. ISBN: 1-85573-600-4, 2002.

[30] J. L. Schulz, B. Command, G. G. Goble, and D. M. Frangopol. *Efficient Field Testing and Load Rating of Short- and Medium-span Bridges.* Structural Engineering Review. South Dakota School of Mines and Technology, 1997.

[31] C. H. Jenkins, L. Kjerengtroen, and H. Oestensen. *Sensitivity of Parameter changes in Structural Damage Detection.* Mechanical Engineering Department. pp. 181-194, 1995.

[32] C. C. Ciang, J. R. Lee, and H. J. Bang. *Structural Health Monitoring for a Wind Turbine System: a Review of Damage Detection methods.* Journal of Measurement Science and Technology,, March 2008.

[33] A.G. Dutton, M.J. Blanch, P. Vionis, D. Lekou, D.R.V. van Delft, P.A. Joosse, A. Anastassopoulos, D. Kouroussis, T. Kossivas, T.P. Philippidis, T.T. Assimakopoulou, G. Fernando, C. Doyle, and A. Proust. *Acoustic Emission Condition Monitoring Of Wind Turbine Rotor Blades: Laboratory Certification Testing To Large Scale In-Service Deployment.* European Wind Energy Conference. European Commission, 2003.

[34] M. J. Blanch and A. G. Dutton. *Acoustic Emission Monitoring of Field Tests of an operating Wind Turbine.* Key Engineering Materials. Vol. 245-246, pp 475-482, 2003.

[35] D. Tcherniak and L. L. Moelgaard. *Active Vibration-based SHM System: Demonstration on an Operating Vestas V27 Wind Turbine.*
PDF:`http://orbit.dtu.dk/files/128004294/32_Tcherniak.pdf`, 2016.

[36] M. D. Ulriksen, D. Tcherniak, and L. Damkilde. *Damage Detection in an Operating Vestas V27 Wind Turbine Blade by use of Outlier Analysis.*
PDF: `http://orbit.dtu.dk/files/128004294/32_Tcherniak.pdf`, 2016.

[37] M. D. Ulriksen, D. Tcherniak, L. M. Hansen, R. J. Johansen, L. Damkilde, and L. Froeyd. *In-situ Damage Localization for a Wind Turbine Blade Through Outlier Analysis of Stochastic Dynamic Damage Location Vector-induced Stress Resultants.*
PDF: `https://core.ac.uk/download/pdf/84002823.pdf`, 2016.

[38] H. Sohn, M. Dzwonczyk, E. G. Straser, A. S. Kiremidjian, K. H. Law, and T. Meng. *An Experimental Study of Temperature Effect on Modal Parameters of the Alamosa Canyon Bridge.* Earthquake engineering % structural dynamics. Vol. 28, No. 8, pp. 879-897, August 1999.

[39] K. Worden, H. Sohn, and C.R. Farrar. *Novelty Detection in a Changing Environment; Regression and Interpolation Approaches.* Journal of Sound and Vibration. Vo. 258 no. 4, pp. 741-761, 2002.

[40] E. J. Cross, K. Worden, and Q. Chen. *Cointegration: A Novel Approach for the Removal of Environmental Trends in Structural Health Monitoring Data.* University of Sheffield, Department of Mechanical Engineering, 2011.

[41] E. J. Cross and K. Worden. *Cointegration and why it works for SHM.* University of Sheffield, Department of Mechanical Engineering, 2012.

[42] E. J. Cross, K. Worden, G. Manson, and S.G. Pierce. *Features for Damage Detection with Insensitivity to Environmental and Operational Variations.* University of Sheffield, Department of Mechanical Engineering, 2012.

[43] G. Manson. *Identifying Damage Sensitive, Environment Insensitive Features for Damage Detection.* Proceedings of IES Conference. Swansea, UK., 2002.

[44] C. Granger and P. Newbold. *Spurious Regressions in Econometrics.* Journal of Econometrics. Vol. 2, No.2, pp. 111-120, July 1974.

[45] Q. Chen, u. Kruger, and A. Leung. *Cointegration Testing Method for Monitoring Nonstationary Processes.* Industrial & Engineering Chemistry Research. Vol. 48 no. 7, pp. 3533-3543., 2009.

[46] D. J. Inman. *Engineering Vibrations, 3rd edition.* Pearson International Edition. ISBN 10: 0132281732, 2007.

[47] S. Setio, H. D. Setio, L. Jezequel, and Ecole Centrale de Lyon. *Modal Analysis of Nonlinear Multi-Degree-of-Freedom Structure.* The International Journal of Analytical and Experimental Modal Analysis. Vo. 7, no. 2, pp 75-93, April 1992.

[48] A. Brandt. *Noise and Vibration Analysis.* John Wile and Sons, Limited. ISBN: 9780470746448, February 2011.

[49] K. Worden, G. Manson, and N. R. J. Fieller. *Damage Detection Using Outlier Analysis.* Journal of Sound and Vibration. Vo. 229 no. 3, pp. 647-667, 2000.

[50] C. Granger and R. Engle. *Co-integration and Error Correction: Representation, Estimation and Testing.* Econometrica. Vol. 55, No.2, pp. 251-276, March 1987.

[51] G. U. Yule. *Why Do We Sometimes get Nonsense-Correlations between Time-Series?–A Study in Sampling and the Nature of Time-Series.* Journal of the Royal Statistical Society. Vol. 89, No.1, pp. 1-63, January 1926.

[52] D. A. Dickey and W. A. Fuller. *Distribution of the Estimators for Autoregressive Time Series With a Unit Root.* Journal of the American Statistical Association. Vol. 74, No. 366 pp. 427-437, June 1979.

[53] S. Johansen. *Modelling of Cointegration in the Vector Autoregressive Model.* European University Institute, Department of Economics. Economic Modelling, pp.359-373, Nov. 1991.

[54] S. Johansen. *Estimation and Hypothesis Testing of Cointegration Vectors in Gaussian Vector Autoregressive Models.* Econometrica. Vol. 89, No.7, pp. 1551-1580, Nov. 1991.

[55] D. Tcherniak and L. L. Moelgaard. *Active Vibration-based SHM System: Application to Wind Turbine Blades.* PDF:`http://orbit.dtu.dk/files/113055156/1742_6596_628_1_012072.pdf`, 2015.

[56] T. V. L. Vo, B. A. Qadri, and S. H. Knudsen. *Udvikling af Analyseredskab, til Brug På Udbardunerede Master (Danish).* Aalborg University, Esbjerg Department. Bachelor Project, 2015.

[57] T. V. L. Vo, B. A. Qadri, S. H. Knudsen, J. Zhebawi, M. S. Grønholdt, and E. Aazam. *Theoretical- and Experimental Study of a Perforated I-beam.* Aalborg University, Esbjerg Department. Bachelor Project, 2015.

[58] R. D. Cook, D. S. Malkus, M. E. Plesha, and R. J. Witt. *Concepts and Applications of Finite Element Analysis.* John Wiley & Sons Inc. 4th Edition. ISBN: 978-0-471-35605-9, 2002.

Appendix **A**

Appendix - Supplementary Analyses

A.I Initiation by means of Finite Element Algorithms

Due to the author's novelty regarding structural health monitoring techniques in the beginning phase of the project, it has been decided, that the creation of numerical damage identification algorithms, has to be initiated based on solid and reliable ground where the author is confident. This can be achieved by constructing codes representing simple finite element scenarios, where the input parameters as well as the introduced damage are completely controllable. Everything is fictional and therefore, the outcome will be predictable verifiable. By doing this, the possibilities of errors in all processes will be narrowed down/eliminated and the theories of which the codes are built on, can be confirmed valid.

The objective of the upcoming cases, is to detect introduced damage based on outlier analyses using Mahalanobis metric, referring to section 4.2 on page 26. As stated the intention is to establish a solid foundation so that this, well-established detection scheme, can be processed and confirmed valid for the author in order to continue employing it. The challenge here, is to fabricate at least two sets of data, of which the Mahalanobis distance can be calculated and compared. One set of data to form the baseline model representing a healthy state and another set of data representing a damaged state. Due to the experience of the author regarding finite element analysis in previous projects, cases based on finite element theory are numerically fabricated and analyzed. The parameter to be investigated, in order to resemble the experimental study of the V27 turbine, is chosen to be acceleration data which is achieved by time integration. Classical beam theory and damping, i.e. Bernoulli Euler's Beam Theory and Rayleigh Damping, have been implemented. The specific composition of these finite element cases such as the implemented physical properties, element topology, the boundary conditions, the applied time integration scheme etc. are summarized in the following section. The underlying fundamental concepts of finite element analysis, for instance the Bernoulli Euler's Beam Theory, the discretization strategy, and the construction and assembly of stiffness-, mass-, and damping matrices, are assumed being in familiar to the reader, hence the details of these are not elaborated in this thesis context. In a contrary case, the reader is recommended to read one of the author's previous reports with the topic of finite element analysis: referring to [56] and [57], or, of course, the reader can read the widely used textbook for engineering as well as educational purposes, namely *"Concepts and Applications of Finite Element Analysis"* authored by Cook et al. (2002) [58].

Three independent codes with gradually increased complexity, i.e. with increasing degrees of freedom (DOF) per node namely, 1-DOF elements, 2-DOF elements and 3-DOF elements, have been created, referring to Figure A.1 and the actual codes can be found in appendix B, in the folders of "MATLAB" → "FEA", named as "FEA1D.m", "FEA2D.m" and "FEA3D.m". The first code only considers 1 degree of freedom (DOF) per node; the axial displacements u, the second code considers 2 DOFs per node; the axial u and the rotational θ displacements, and the third code considers 3 DOFs per node; the axial u, transversial v and the rotational θ displacements.

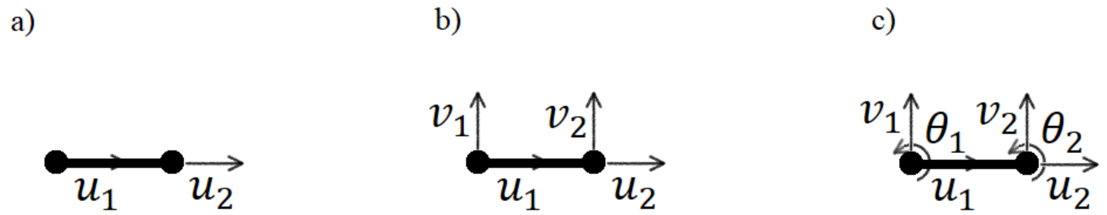

Figure A.1: Illustration of the element types and the respective degrees of freedom for each code. a) FEA1D, b) FEA2D, c) FEA3D.

.

The approach is to apply an initiating force, inducing vibrational response in the structure, for each type of degree of freedom. In other words, an axial force u, a transverse force v and a rotational force θ has been initiated respectively in the three respective codes. A cantilever beam system consisting of 5 elements is composed as illustrated in Figure A.2, in all three cases.

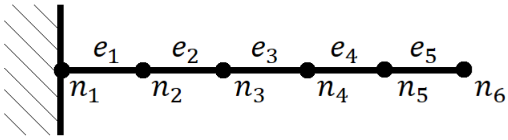

Figure A.2: Illustration of the nodal and elemental topology for all three cases.

.

Node 1 is fixed against displacement in all three cases, and the initial force is applied on Node 6. The material properties is chosen according to conventional steel, i.e. Young's Modulus, $E = 210GPa$ and density, $\rho = 7.850kg/m^3$.

The first set of "undamaged" data, forming the baseline training data, is calculated with the boundary conditions as stated without any further adjustments. The "damage", to be detected by outlier analysis, is introduced by reducing Young's Modulus. Subsequently, white Gausian noise is added respectively to the two data sets, in order to achieve variational data for visual purposes as well as to mimic and represent random natural processes in practical cases. The results of these fabricated cases, in form of semi-logarithmic plots, are presented in Figure A.3. The actual numerical codes can be found in the attached CD, referring to Appendix A in the folders of "MATLAB" $\rightarrow$ "FEA" and named as "FEA1D.m", "FEA2D.m" and "FEA3D.m".

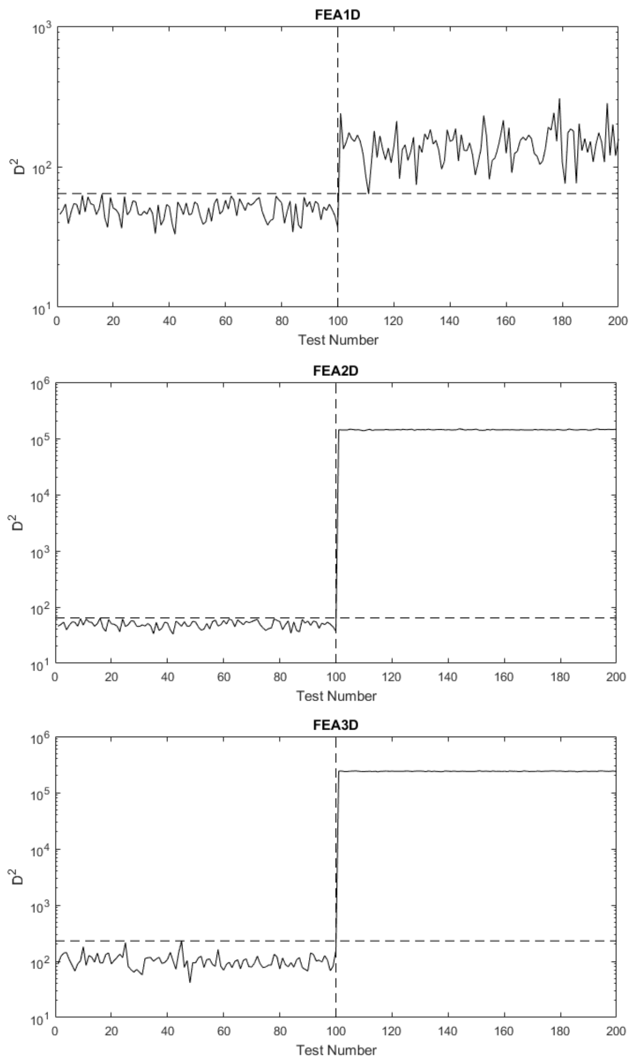

Figure A.3: Semi-logarithmic plots of outlier analysis results of the three FEA cases. The horizontal dashed lines mark the threshold, ϑ, and the vertical dashed lines separate the two states of healthy and damaged, after 100 number of tests.

.

Based on the results in Figure A.3, it can be observed, that the Mahalanobis metric provides the capability to distinguish between healthy and damaged states. The first 100 test numbers represent the healthy state, and the test numbers of 100-200, represent the damaged state. For all three cases, the D^2distance within the damage state exceeds the threshold.

In addition to the three 5-element cantilever beam cases, a fourth case consisting of 11 elements is constructed. This case is composed as a truss structure as illustrated in Figure A.4.

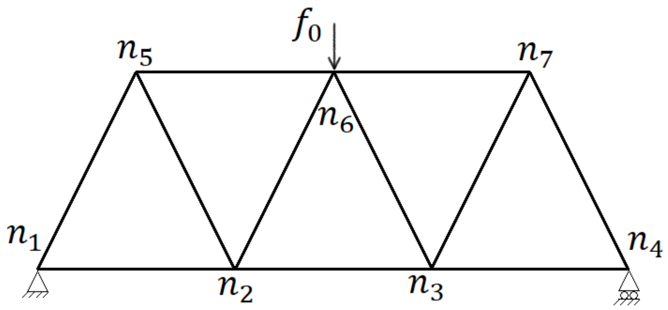

Figure A.4: The truss structure including boundary conditions, nodal number and location of initial force.

.

The purpose of this case is to eliminate errors in the code such as errors in the assembly of stiffness matrices or in the coordinate orientation and transformations, since, the truss structure includes angular rotations of elements as well as joints with 3 elements instead of 2. The boundary conditions are depicted in Figure A.4, where the transversial force, f_0, is implemented to induce response of the structure. In a similar manner as the previous cases, the approach here, is to firstly, calculate the responses of the structure, and secondly, reduce Young's modulus and recalculate the responses. The two sets of data can subsequently be inputs for the damage detection scheme. The results of the outlier analysis based on Mahalanobis metric is presented in Figure A.5. The actual code is to be found in Appendix B, named "FEA3Dtruss.matlab".

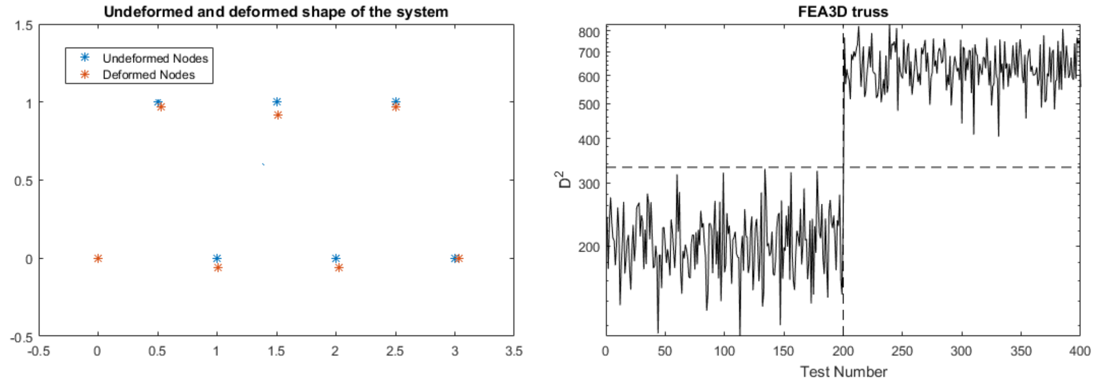

Figure A.5: Nodal deformation plot (scaled) and Semi-logarithmic plot of outlier analysis results for the truss case. The horizontal dashed line marks the threshold, ϑ, and the vertical dashed line separates the two states of healthy and damaged, after 200 number of tests.

.

The nodal deformations as well as the outlier analysis are presented and the results are evaluated as acceptable. As observed, the scheme is capable of detecting a change in the physical properties, resulting in outlying values between the test numbers 200-400, where "damage", i.e. reduction of Young's modulus, is present. These results were expected in advance, hence, the FEA codes are confirmed acceptable for now and the detection scheme can be used and improved further.

Appendix B

Appendix - Attached CD Including Developed Algorithms

Contents of digital data and related formats stored in the attached disc:

- Complete report in *.pdf-format*
- 'MATLAB'. Folder with numerical Matlab algorithms including following subfolders:
  - 'FEA'
    Finite element algorithms in *.m-format*
  - 'DETECTION'
    Damage detection algorithms based on Mahalanobis metric in *.m-format*
  - 'COINTEGRATION'
    Cointegration algorithms in *.m-format*
  - 'EXPERIMENT'
    Algorithms employing experimental data providing results in *.m-format*
  - 'FILES FOR LOADING'
    Files with empirical data etc. in *.mat-format*